

# Estimating degree-day factors of snow based on energy flux components

Muhammad Fraz Ismail <sup>1,2</sup>, Wolfgang Bogacki <sup>2</sup>, Markus Disse <sup>1</sup>, Michael Schäfer <sup>2,3</sup> and Lothar Kirschbauer <sup>2</sup>

5 <sup>1</sup> TUM School of Engineering and Design, Technical University of Munich, Germany

<sup>2</sup> Department of Civil Engineering, Koblenz University of Applied Sciences, Germany

<sup>3</sup> Faculty of Agriculture, Yamagata University, Tsuruoka, Japan

**Correspondence:** Muhammad Fraz Ismail (fraz.ismail@tum.de; ismail@hs-koblenz.de)

## 10 Abstract

Meltwater from mountainous catchments dominated by snow and ice is a valuable source of fresh water in many regions. At mid-latitudes, seasonal snow cover and glaciers act like a natural reservoir by storing precipitation during winter and releasing it in spring and summer. Snowmelt is usually modelled either by energy balance or by temperature-index approaches. The energy balance approach is process-based and more sophisticated but requires extensive input data, while the temperature-index approach uses the degree-day factor (*DDF*) as key parameter to estimate melt of snow and ice merely from air temperature. Despite its simplicity, the temperature-index approach has proved to be a powerful tool for simulating the melt process especially in large and data scarce catchments.

The present study attempts to quantify the effects of spatial, temporal, and climatic conditions on the *DDF* of snow in order to gain a better understanding of which influencing factors are decisive under which conditions. The analysis is based on the individual energy flux components, however formulas for estimating the *DDF* are presented to account for situations where observed data is limited. A detailed comparison between field-derived and estimated *DDF* values yields a fair agreement with bias = 0.14 mm  $^{\circ}\text{C}^{-1} \text{d}^{-1}$  and Root Mean Square Error (RMSE) = 1.12 mm  $^{\circ}\text{C}^{-1} \text{d}^{-1}$ .

25 The analysis of the energy balance processes controlling snowmelt indicates that cloud cover and snow albedo under clear sky are the most decisive factors for estimating the *DDF* of snow. The results of this study further underline that the *DDF* changes as the melt season progresses and thus also with altitude, since melting conditions arrive later at higher elevations. A brief analysis of the *DDF* under the influence of climate change shows that the *DDFs* are expected to decrease when comparing periods of similar 30 degree-days, as melt will occur earlier in the year when solar radiation is lower and albedo is then likely to be higher. Therefore, the *DDF* cannot be treated as a constant parameter especially when using temperature-index models for forecasting present or predicting future water availability.

**Keywords:** Degree-Day Factor, Snowmelt, Energy balance, Temperature-Index, Climate change

35 **1. Introduction**

Meltwater from snow and ice dominated mountainous basins is a main source of fresh water in many regions (Immerzeel et al., 2020). Seasonal snow cover and glaciers act as natural reservoirs which significantly affect catchment hydrology by temporarily storing and releasing water on various time scales (Jansson et al., 2003). In such river basins, snow and glacier melt runoff modelling is a valuable 40 tool when predicting downstream river flow regimes, as well as when assessing the changes in the cryosphere associated with climate change (Hock, 2003; Huss and Hock, 2018). Therefore, a more accurate quantification of the snow and ice melt processes and related parameters is the key to a successful runoff modelling of present and future water availability.

Two different approaches are common in snowmelt modelling. The energy balance approach is process- 45 based but data-intensive, since melt is deduced from the balance of in- and outgoing energy components (Braithwaite, 1995a; Arendt and Sharp, 1999). On the contrary, temperature-index or also-called degree-day models merely use the air temperature as an index to assess melt rates (Martinec, 1975; Bergström, 1976; Quick and Pipes, 1977; DeWalle and Rango, 2008). The degree-day approach is very common and popular since air temperature is an excellent surrogate variable for the energy available in near- 50 surface atmosphere that governs the snowmelt process (Lang and Braun, 1990). The relationship between temperature and melt is defined by the degree-day factor (*DDF*) (Zingg, 1951; Braithwaite, 2008), which is the amount of melt that occurs per unit positive degree-day (Braithwaite, 1995a; Kayastha et al., 2003; Martinec et al., 2008). There are different methods by which the *DDF* can be determined, e.g. by measurements using ablation stakes (Zhang et al., 2006; Muhammad et al., 2020), 55 using snow lysimetric outflows (Kustas et al., 1994), by estimating daily changes in the snow water equivalent (Martinec, 1960; Rango and Martinec, 1979, 1995; Kane et al., 1997), or using satellite based snow cover data (Asaoka and Kominami, 2013; He et al., 2014).

The *DDF* is usually treated as a decisive parameter subject to model calibrations because sufficient direct observations are typically lacking in large catchments. Most commonly, for calibrating the *DDF*, 60 runoff is used (Hinzman and Kane, 1991; Klok et al., 2001; Luo et al., 2013; Bogacki and Ismail, 2016). However, it is also important to note that the calibration of the *DDF* using runoff can be significantly affected by other model parameters due to their interdependency (Gafurov, 2010; He et al., 2014). Researchers also select *DDF* directly from other studies, hence the spatial transferability is not always 65 good (e.g. Carenzo et al., 2009; Wheler, 2009). Despite its simplicity, this approach has proved to be a powerful tool for simulating the complex melt processes especially in large and data scarce catchments (Zhang et al., 2006; Immerzeel et al., 2009; Tahir et al., 2011; Lutz et al., 2016).

Extensive research has been devoted to the enhancement of the original degree-day approach. Braun, (1984) introduced the Temperature-Wind-Index method by the inclusion of a wind-dependent scaling factor. A hybrid approach, which combines both, temperature-index and energy balance methods was 70 introduced by Anderson, (1973). Oerlemans, (2001) introduced a simplified energy balance approach.

Hock, (1999) attempted to improve the simple temperature-index model by adding a term to consider potential incoming direct solar radiation for clear sky conditions. The potential clear sky solar radiation is calculated as a function of the position of the sun, geographic location and a constant atmospheric transmissivity (Hock and Noetzli, 1997; Hock, 1999). This model is comparable with the data requirements of a simple degree-day model. Pellicciotti et al., (2005) considered the net shortwave radiation instead of just incoming shortwave radiation by including snow albedo in their proposed degree-day model. Although all these enhancements focus on adding more physical foundation to the original degree-day method, the classical approach is still more popular because of its simplicity and merely dependence on air temperatures.

75 A weakness of the degree-day approach is the fact that it works well over longer time periods (e.g. 10-daily, monthly, seasonal) but with increasing temporal resolution, in particular for sub-daily time-steps, the accuracy decreases (Lang, 1986; Hock, 1999). In addition, the spatial variability of melt rates is not modelled accurately as the *DDFs* are usually considered invariant in space. However, melt rates can be subject to substantial small-scale variations, particularly in high mountain regions due to topography

85 (Hock, 1999). For example, topographic features (e.g. topographic shading, aspect and slope angles) including altitude of a basin can influence the spatial energy conditions for snowmelt and lead to significant variations of the *DDF* (Hock, 2003; Marsh et al., 2012; Bormann et al., 2014). Under otherwise similar conditions, *DDFs* are expected to increase with (i) increasing elevation, (ii) increasing direct solar radiation input and (iii) decreasing albedo (Hock, 2003).

90 Obviously, the *DDF* cannot be treated as a constant parameter as it varies due to the changes in the physical properties of the snowpack over the snowmelt season (Rango and Martinec, 1995; Prasad and Roy, 2005; Shea et al., 2009; Martinec et al., 2008; Ismail et al., 2015; Kayastha and Kayastha, 2020). The spatio-temporal variation in the *DDF* (Zhang et al., 2006; Asaoka and Kominami, 2013) not only affects the accuracy of snow and ice melt modelling (Quick and Pipes, 1977; Braun et al., 1993;

95 Schreider et al., 1997) but also is a key to estimate heterogeneity of the snowmelt regime (Hock, 1999, 2003; DeWalle and Rango, 2008; Braithwaite, 2008; Schmid et al., 2012). Since melt depends on energy balance processes and topographic settings, changes in *DDFs* are a result of energy components that vary with different climatic conditions (Ambach, 1985; Braithwaite, 1995a). Another topic that needs attention is the stationarity of the *DDF* under climate change (Matthews and Hodgkins, 2016).

100 Moreover, it is important to consider the over-sensitivity of temperature-index models, often used by large-scale studies, to future warming (Bolibar et al., 2022; Vincent and Thibert, 2022). Future water availability under climate change scenarios is typically modelled with *DDFs* calibrated for the present climate, which increases the parametric uncertainty introduced by the hydrological models (Lutz et al., 2016; Ismail and Bogacki, 2018; Hasson et al., 2019; Ismail et al., 2020).

105 In order to allow for a more process-based estimate of the *DDF*, present study attempts to quantify the contribution of each energy balance component to snow melt and subsequently to the overall *DDF*. Considering that degree-day models are typically utilised in large catchments with data scarce

conditions, we estimate energy balance components by formulas with minimum data requirement following the approach by Walter et al., (2005). Based on these formulas, the *DDF* contribution 110 corresponding to the respective energy components is quantified in tables and graphs for common snowmelt conditions, which can be used for a rapid appraisal. The presented approach is open in the sense that if for any of the energy balance components observed data is available, or more sophisticated models are desired, these can easily replace each of the presented approximations.

The objective of this study is not to incorporate an energy balance based *DDF* approach into 115 temperature-index models, but rather to gain a quantitative insight on how different factors affect the *DDF*. Through this approach, we aim to obtain a good estimate and realistic limits for calibration of the *DDF* parameter and as to predict changes during the melt season for forecasting purposes or to study the effects of climate change.

## 2. Test site and datasets

### 120 2.1 Test Site

The test site locates in the Dreisäulerbach catchment, which is a part of the Isar River system and lies in the sub-alpine region of Bavaria in the Ammergauer Alps, Germany. The Dreisäulerbach catchment approximately lies between latitudes  $47^{\circ}34'55''$ – $47^{\circ}35'05''$  North and longitudes  $10^{\circ}56'40''$ – $10^{\circ}57'07''$  East. It covers an area of about  $2.3 \text{ km}^2$  and has a mean hypsometric elevation of just over 1200 m a.s.l. 125 (Figure 1). The elevation ranges from about 950 m a.s.l. at Linderhof gauging station up to 1768 m a.s.l. at the Hennenkopf.

The area is mostly characterized by south facing slopes, but also contains northern slopes in southern parts of the catchment. The catchment is densely forested which during the winter season is fully snow-covered. The mean annual temperature in the observation period (i.e. November 2016 – May 2021) is 130 about  $5.8^{\circ}\text{C}$  and the long-term (i.e., 1961 – 2018) mean annual precipitation at the Ettal-Linderhof station of the Water Science Service Bavaria is reported to be 1676 mm (Kopp et al., 2019).

In order to observe the seasonal snow dynamics, snow measurement instruments in addition to a standard meteorological station have been installed at the Brunnenkopfhütte test site at an elevation of 1602 m a.s.l. (see Figure 2). The installed station has various sensors that measure temperature, pressure, wind, 135 solar radiation (incoming, outgoing), snow depth, snow scale, a snowpack analyser and a pluviometer. Table 1 summarises the observed monthly meteorological data at Brunnenkopfhütte station. Figure 3 presents the observed snow water equivalent (SWE) at the test site.

**Table 1** Observed monthly average meteorological data at Brunnenkopfhütte (November 2016 – May 2021)

Variables <sup>1</sup>	Jan	Feb	Mar	Apr	May	Jun	Jul	Aug	Sep	Oct	Nov	Dec
$T_a$ (°C)	-2.48	-0.41	0.52	4.14	6.76	12.40	13.62	14.22	9.69	7.72	3.06	0.08
$P$ (mm)	230.2	147.3	138.8	115.1	188.0	185.4	216.5	241.5	183.7	162.4	107.2	195.9
$u$ (ms <sup>-1</sup> )	1.08	1.01	1.10	0.97	0.71	0.60	0.59	0.59	0.60	0.79	1.02	1.00
$RH$ (%)	74.2	69.3	73.4	72.2	82.1	78.2	76.7	78.1	82.8	71.7	70.5	69.4
$A$ (-)	0.80	0.74	0.69	0.51	0.42	—	—	—	—	—	0.45	0.72
$K_T$ (-)	0.51	0.52	0.53	0.53	0.40	0.43	0.43	0.45	0.48	0.55	0.50	0.49
$SR_{in}$ (W m <sup>-2</sup> )	61	97	148	200	181	207	200	185	150	119	68	51

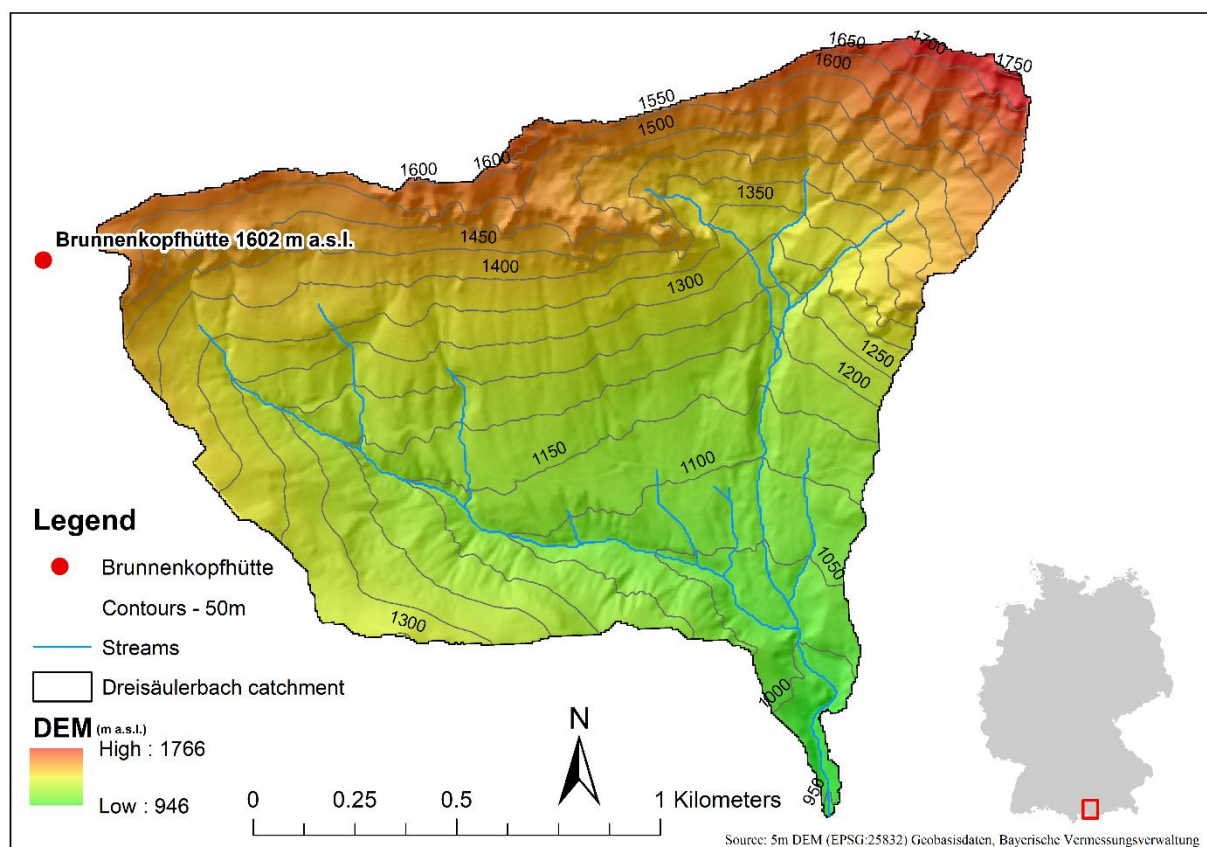


**Figure 1** Location of Brunnenkopfhütte automatic snow and weather station in the Dreisäulerbach catchment – German Alps

<sup>1</sup>  $T_a$  = Air temperature

$P$  = Precipitation

$u$  = Wind speed

$RH$  = Relative Humidity

$A$  = Albedo (only considered when ground is snow covered)

$K_T$  = Clearness index

$SR_{in}$  = Incoming shortwave radiation

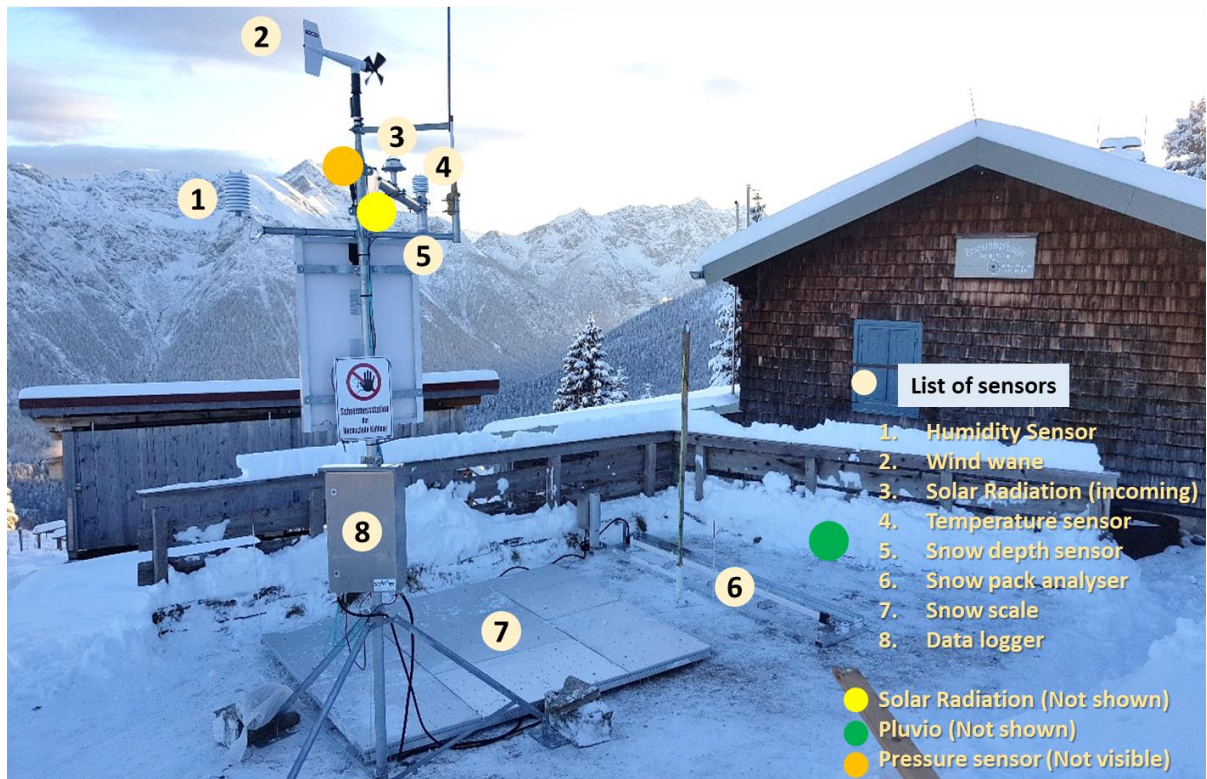


**Figure 2** Automatic snow and weather station at Brunnenkopfhütte, 1602 m a.s.l. (Image credit – Wolfgang Bogacki)

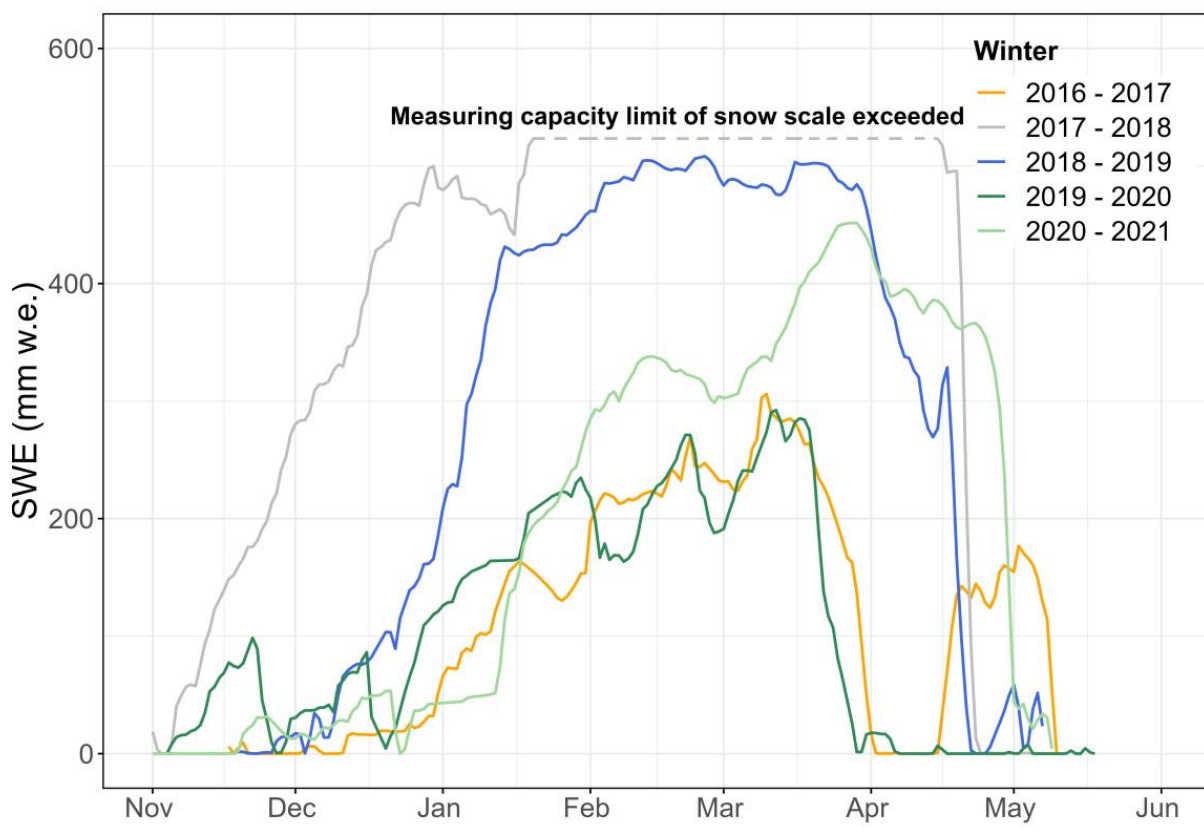


**Figure 3** Observed SWE (mm) at the Brunnenkopfhütte snow station (period: Winter 2016/2017 – 2020/2021)

## 2.2 Datasets

The Present study utilises three different datasets. Data sources as well as aim of using these datasets  
155 are mentioned as follow:

1. We use observed hydro-meteorological datasets from a test site (i.e., Brunnenkopfhütte) with the aim to show how the *DDF* of snow can be estimated for a specific site under naturally varying hydro-meteorological conditions.
2. In order to demonstrate the variation of the *DDF* over time, location, and altitude, as well as its  
160 significance for temperature-index modelling, we use elevation-zone temperature data of the Upper Jhelum Basin from a previous study (Bogacki and Ismail, 2016).
3. In the discussion section (Sec. 5), we perform a brief analysis in order to show the influence of climate change on the *DDF* in poorly monitored regions. In this specific analysis, projected  
165 changes in temperature are based on a previous study (Ismail et al., 2020). These projected changes in temperature are the median of four GCMs (GFDL-ESM2M, HadGEM2-ES, IPSL-CM5A-LR, and MIROC5) that are driven by two representative concentration pathways (RCP2.6 and RCP8.5). This data is provided by the Inter-Sectoral Impact Model Intercomparison Project (ISIMIP) (Hempel et al., 2013; Frieler et al., 2017).

## 3. Materials and methods

170 The primary objective of this paper is to analyse the contribution of individual energy balance components to snowmelt, in order to better understand and predict, how the lumped degree-day factor will vary with the season, latitude, altitude, and the actual meteorological conditions. In addition, we want to demonstrate following the approach of Walter et al., (2005), how these energy balance components can be estimated with minimal data requirements, as limited data availability is the major  
175 reason to apply temperature-index models.

### 3.1 Degree-Day Factor

The basic formulation of the degree-day method calculates daily snowmelt depth  $M$  (mm) by multiplying the number of degree-days  $T_{DD}$  ( $^{\circ}\text{C d}$ ) with the degree-day factor  $DDF$  ( $\text{mm } ^{\circ}\text{C}^{-1} \text{ d}^{-1}$ ) (Zingg, 1951; Braithwaite, 1995a; Rango and Martinec, 1995).

$$M = DDF \times T_{DD} \quad (1)$$

180 Degree-days  $T_{DD}$  are only defined if a characteristic air temperature lies above a reference temperature  $T_0$ ; otherwise,  $T_{DD}$  is set to  $0^{\circ}\text{C d}$ . Typically, the freezing point  $T_0 = 0^{\circ}\text{C}$  is chosen as reference temperature (DeWalle and Rango, 2008). Depending on the availability of temperature data, the characteristic air temperature is usually calculated as the mean of maximum and minimum daily air temperatures (Braithwaite, 1995a) or the mean of hourly observations (Rango and Martinec, 1995; 185 DeWalle and Rango, 2008). Other approaches like daily maximum temperature (Bagchi, 1983),

integrating the positive part of a diurnal cycle (Ismail et al., 2015) or averaging the positive degree-day sum of  $m$  daily observations (Braithwaite and Hughes, 2022) are also common.

By a simple re-arrangement of eq. (1) to

$$DDF = \frac{M}{T_{DD}} \quad (2)$$

the  $DDF$  can be calculated for given degree-days  $T_{DD}$ , if the daily melt depth  $M$  is known either by observation or by calculation. Likewise, the portion of the degree-day factor  $DDF_i$  associated to the melt depth  $M_i$  which relates to any of the individual energy balance components (see eq. (4)), can be determined.

The energy needed to melt ice at 0°C into liquid water at 0°C is defined by the latent heat of fusion of ice (333.55 kJ kg<sup>-1</sup>). Thus the melt depth  $M_i$  caused by an energy flux  $Q_i$  (W m<sup>-2</sup>) over a certain time-period  $\Delta t$  (s) can be calculated from the relation (USACE, 1998; Hock, 2005)

$$M_i = \frac{Q_i}{\lambda \rho_w} \Delta t \cong 3.00 \times 10^{-6} Q_i \Delta t \quad (3)$$

where  $\rho_w$  is the density of water at 0°C (999.84 kg m<sup>-3</sup>). In the context of degree-day factor models, the time-period  $\Delta t$  is usually taken as 1 day = 86400 s, though some authors (Hock, 1999; McGinn, 2012) have calculated degree-day factors also for sub-daily, e.g. hourly periods. According to the relation given in eq. (3), an energy flux of 1 W m<sup>-2</sup> for a single day will result in a melt depth of 0.26 mm.

## 200 3.2 Energy Balance

The energy flux available for snowmelt  $Q_M$  can be calculated from the balance of energy fluxes entering or leaving the snowpack and the change in the internal energy stored in the snowpack  $\Delta Q$  (e.g. USACE, 1998)

$$Q_M = Q_S + Q_L + Q_H + Q_E + Q_G + Q_P - \Delta Q \quad (4)$$

where  $Q_S$  and  $Q_L$  are the net short- and longwave radiation,  $Q_H$  is the sensible heat,  $Q_E$  the latent energy of condensation or vaporization,  $Q_G$  the heat conduction from the ground, and  $Q_P$  the energy contained in precipitation (all terms in W m<sup>-2</sup>).

In the following sections, the individual components of the energy balance are discussed in more detail. As heat conduction from the ground into the snowpack is small and can be in general neglected except when first snow falls on warm ground (Anderson, 2006), the component  $Q_G$  is not considered in the further analysis.

### 3.2.1 Shortwave Radiation

Shortwave radiation emitted from the sun is usually the largest source of energy input to the snowpack. The net energy flux  $Q_s$  ( $\text{W m}^{-2}$ ) entering the snowpack by absorption of shortwave radiation is

$$Q_s = (1 - A)S_i \quad (5)$$

where  $A$  is the snow albedo (–) and  $S_i$  the incident solar radiation ( $\text{W m}^{-2}$ ) on the snow surface. A widely used approach (Masters, 2004; Yang and Koike, 2005; Badescu, 2008) to determine the incident solar radiation on Earth's surface is the introduction of a clearness index  $K_T$  (–)

$$S_i = K_T S_0 \quad (6)$$

where  $S_0$  is the mean daily potential extra-terrestrial solar radiation ( $\text{W m}^{-2}$ ) that would insolate a horizontal surface on the Earth's ground if no atmosphere would be present.

#### Potential insolation at the top of atmosphere

The potential insolation, which is only dependent on the changing position of the sun during the year in relation to the geographic location of the incident point on the Earth's surface, can be calculated from the equation (Masters, 2004)

$$S_0 = G_s \frac{1}{d_r^2} \frac{1}{\pi} (\cos(\phi) \cos(\delta) \cos(\omega_s) + \omega_s \sin(\phi) \sin(\delta)) \quad (7)$$

where  $G_s$  is the solar constant ( $\text{W m}^{-2}$ ),  $d_r$  the relative distance earth to sun (–),  $\phi$  the geographic latitude (rad) of the incident point,  $\delta$  the solar declination (rad), and  $\omega_s$  the sunrise hour angle (rad). The solar constant  $G_s$  is slightly varying with the occurrence of so-called sunspots. Measurements by Kopp and Lean, (2011) indicate a present value of about  $1361 \text{ W m}^{-2}$ .

Both sun position variables, the relative distance Earth to sun, and the solar declination, can be calculated quite exactly by rigorous astronomical algorithms (Meeus, 1991; Reda and Andreas, 2004) but for non-astronomical purposes, more simple formulas are sufficiently accurate. The relative distance Earth to sun, which is varying over the year due to the elliptical orbit of the earth, can be approximated by (Masters, 2004)

$$\frac{1}{d_r^2} \approx 1 + 0.034 \cos\left(\frac{2\pi J}{365}\right) \quad (8)$$

where  $J$  is the day number, with  $J = 1$  on January 1<sup>st</sup>. The solar declination can be obtained from the sinusoidal relationship

$$\delta \approx 0.409 \sin\left(\frac{2\pi}{365}(J - 81)\right) \quad (9)$$

that puts the spring equinox on day  $J = 81$ . Knowing the solar declination  $\delta$ , the sunrise hour angle  $\omega_s$

235 can be calculated from

$$\cos \omega_s = -\tan(\phi) \tan(\delta) \quad (10)$$

On the northern hemisphere the maximum extra-terrestrial radiation occurs at the summer solstice with a fairly identical mean daily energy flux of about  $480 \text{ W m}^{-2}$  over latitudes  $30^\circ - 60^\circ$  North, as the sun's lower altitude angle at higher latitudes is compensated by longer daylight hours. On the contrary, minimum extra-terrestrial radiation at the winter solstice varies strongly with latitude, e.g.,  $227 \text{ W m}^{-2}$  at  $30^\circ$  and only  $24 \text{ W m}^{-2}$  at  $60^\circ$  North.

240

### Clearness Index

When the solar radiation passes through the atmosphere, it is partly scattered and absorbed. While even on a clear day only about 75% of the incoming radiation reaches the ground, by far the largest reflection is caused by clouds. A vast number of solar radiation models exist that parameterise this effect, which 245 is denoted as clearness index  $K_T$  or atmospheric transmissivity  $\tau$ , as a function of meteorological variables. For a review see e.g. Evrendilek and Ertekin (2008), Ahmad and Tiwari (2011), or Ekici (2019).

A fundamental and widely used solar radiation model that is proposed in the context of evapotranspiration calculations (Allen et al., 1998) is the Ångström-Prescott model, which relates the 250 clearness index to the relative sunshine duration

$$K_T = \frac{S_i}{S_0} = a + b \frac{n}{N} \quad (11)$$

where  $n$  is the actual and  $N$  the maximal possible duration of sunshine (hr), where the latter can be calculated from the sunrise hour angle  $\omega_s$

$$N = \frac{24}{\pi} \omega_s \quad (12)$$

The parameters  $a$  and  $b$  in eq. (11) are regression parameters, that usually have to be fitted to observed 255 global radiation. In case no actual solar radiation data is available, the values  $a = 0.25$  and  $b = 0.50$  are recommended (Allen et al., 1998). Though the Ångström-Prescott model has the disadvantage that the parameters have to be fitted and the actual duration of sunshine has to be observed, it has the benefit that both parameters allow for a direct physical interpretation. The parameter  $a$  represents the clearness index  $K_T$  on overcast days ( $n = 0$ ), while their sum  $a + b$  gives the clearness index on clear days ( $n = N$ ).

Commonly remote mountainous regions, only temperature data is available, due to which another group 260 of solar radiation models is typically utilized. In these approaches the difference between daily maximum and minimum air temperature  $\Delta T$  ( $^\circ\text{C}$ ) is used as a proxy for cloud cover, as clear sky

conditions result in a higher temperature amplitude between day and night compared to overcast conditions. Typical models are the exponential approach proposed by Bristow and Campbell (1984) and its later modifications or the simple empirical equation by Hargreaves and Samani (1982)

$$K_T = k_H \sqrt{\Delta T} \quad (13)$$

265 with the empirical coefficient  $k_H = 0.16$  for inland and  $k_H = 0.19$  for coastal locations. Since the influence of cloud cover on the clearness index and thus on the *DDF* can be illustrated much more directly by Ångström-Prescott type models, this model type is further on used in the paper.

270 It is obvious that the attenuation of extra-terrestrial solar radiation is a function of the distance the rays have to travel through the atmosphere, as absorption and scattering occurs all along the way. Several solar radiation models consider altitude as a variable, of which the models below were calibrated including high altitude stations and are of Ångström-Prescott type, thus the altitude effects can be compared directly.

Jin et al. (2005):

$$(a) \quad K_T = (0.0855 + 0.0020\phi + 0.030z) + 0.5654 \frac{n}{N} \quad (14)$$

$$(b) \quad K_T = (0.1094 + 0.0014\phi + 0.0212z) + (0.5176 + 0.0012\phi + 0.0150z) \frac{n}{N} \quad (15)$$

Rensheng et al. (2006):

$$K_T = (0.122 + 0.001\phi + 0.0257z) + 0.543 \frac{n}{N} \quad (16)$$

275 Liu et al. (2019):

$$K_T = (0.1755 + 0.0136z) + (0.5414 + 0.0117z) \frac{n}{N} \quad (17)$$

For all models,  $z$  is the altitude (km) and  $\phi$  the latitude (deg). In eq. (14) and (16) only the parameter  $a$  of eq. (11) is a function of altitude  $z$ , while in eq. (15) and (17) also the parameter  $b$  is dependent on  $z$ .

In order to evaluate the altitude effect separately from other parameters, the clearness index  $K_T$  is split into two components

$$K_T = K_{T_0} \cdot K_z \quad (18)$$

280 where  $K_{T_0}$  is the clearness index at  $z = 0$  m a.s.l. and  $K_z$  is a clearness altitude factor (–) which represents the increase of  $K_T$  with altitude relative to  $K_{T_0}$ . At sea level,  $K_z = 1$  for all models and all values of relative sunshine duration  $n/N$ . Though the clearness altitude factors  $K_z$  obtained from eq. (14) – (17)

are different for each model, they all show a linear increase with altitude, the slope of which depends on the cloudiness (see Figure 4). It should be noted, that although  $K_z$  is higher for overcast than for clear 285 sky conditions, the absolute increase of the clearness index  $K_T$  with altitude is higher under clear sky conditions because of the higher base value  $K_{T_0}$ . For example, at  $z = 2000$  m a.s.l. model Jin (b) (eq. 290 (15)) has a clearness altitude factor  $K_z$  of 1.27 for overcast and 1.10 for clear sky conditions. However, when multiplying by the respective clearness factors at sea level  $K_{T_0}$  of 0.15 and 0.72, the resulting clearness indices  $K_T$  at  $z = 2000$  m a.s.l. increase by 0.04 under overcast and 0.07 under clear sky conditions to an absolute value of 0.19 and 0.79 respectively.

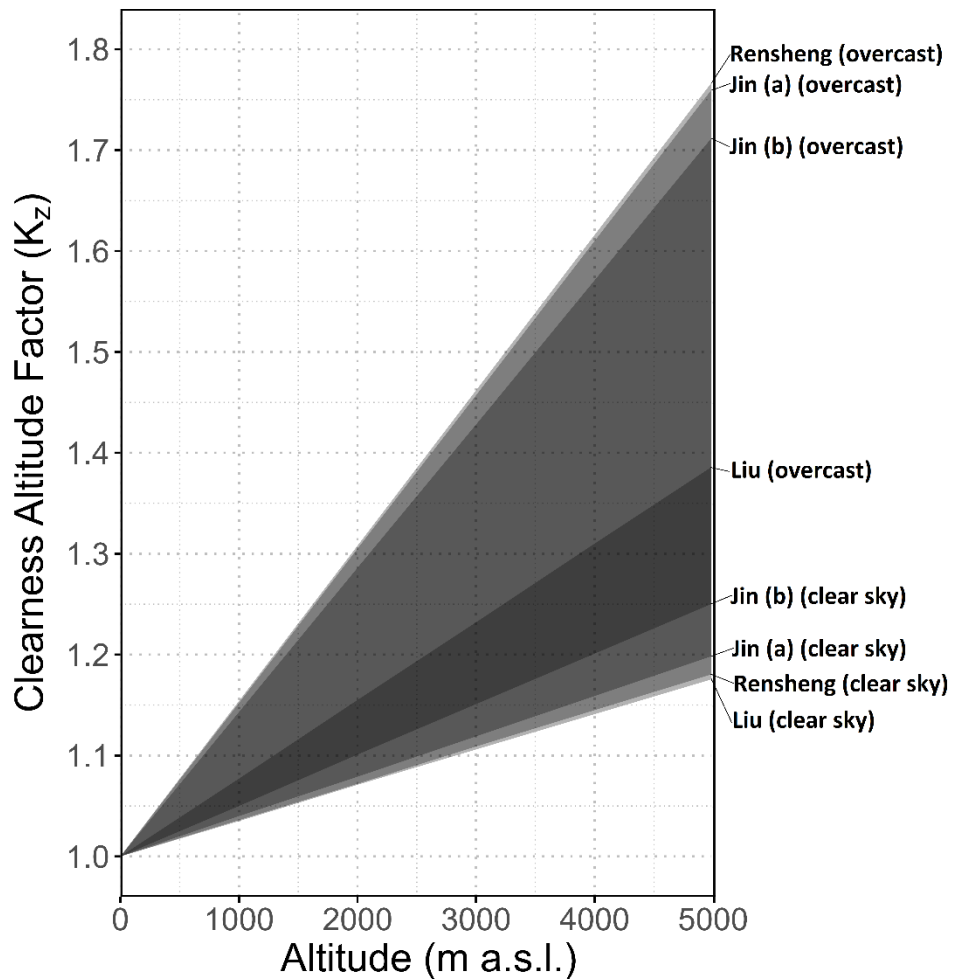


Figure 4 Clearness altitude factor  $K_z$  for latitude  $45^\circ$  and different altitudes, based on different models presented in equations (14 – 17, i.e., Jin (a), Jin (b), Rensheng, and Liu)

## Albedo

295 While the albedo of fresh snow is well above 0.9 (Hock, 2005), indicating that most of the shortwave radiation is reflected, it may drop significantly within a few days due to snow metamorphism. Well aged snow generally has an albedo in the range of 0.4 – 0.5 (Anderson, 2006). Snow albedo is primarily

dependent on the grain size of the snow crystals near the surface but also on aerosols in the snow and dust deposits. Respective snow albedo models are proposed e.g. by Wiscombe and Warren (1980),

300 Warren and Wiscombe (1980) or Amaral et al., (2017). However, because of their data requirements, rather surrogate exponential decay models as formulated by USACE, (1956) are commonly in use, which assumes the decrease of albedo as a function of time after the last significant snowfall. For example Walter et al., (2005) use the empirical relationship

$$A_n = 0.35 - (0.35 - A_{max}) \cdot \exp \left[ - \left( 0.177 + \ln \left( \frac{A_{max} - 0.35}{A_{n-1} - 0.35} \right)^{2.16} \right) \right]^{0.46} \quad (19)$$

where  $A_{n-1}$  is the albedo of the previous day and  $A_{max}$  is the maximum albedo (~0.95) of fresh snow.

305 Following eq. (19), the snow albedo will decrease from 0.95 to 0.52 after 10 days and to 0.43 after 30 days if no new snowfall occurs.

### 3.2.2 Longwave Radiation

The net longwave radiation flux over the snow surface  $Q_L$  ( $\text{W m}^{-2}$ ) is the balance between incoming longwave radiation that is emitted by the atmosphere  $Q_{L,in}$  ( $\text{W m}^{-2}$ ) and outgoing radiation from the 310 snowpack  $Q_{L,out}$  ( $\text{W m}^{-2}$ ).

$$Q_L = Q_{L,in} - Q_{L,out} \quad (20)$$

Longwave radiation is a function of the temperature of the emitting body and can be calculated with the Stefan-Boltzmann law

$$L = \varepsilon \sigma T^4 \quad (21)$$

where  $L$  is the radiative flux ( $\text{W m}^{-2}$ ),  $\varepsilon$  and  $T$  are the emissivity (–) and the absolute temperature (K) of the emitting body, respectively, and  $\sigma$  is the Stefan-Boltzmann constant ( $5.67 \times 10^{-8} \text{ W m}^{-2} \text{ K}^{-4}$ ).

315 In particular fresh snow is nearly a perfect blackbody with respect to longwave radiation with a high emissivity of 0.99 (Warren, 1982; USACE, 1998; Anderson, 2006). For old snow, Brutsaert (1982) gives an emissivity value of 0.97. Given a melting snowpack having a surface temperature of 0°C, the outgoing energy flux can be taken as constant with  $Q_{L,out} \sim 310 \text{ W m}^{-2}$ .

For the atmospheric longwave radiation, usually the air temperature  $T_a$  (K) is used in eq. (21). However, 320 while the snowpack longwave emissivity is virtually constant, the emissivity of the atmosphere is highly variable. Typical values under clear sky conditions range from 0.6 – 0.8, primarily depending on air temperature and humidity (Anderson, 2006) whereas for overcast conditions it can be close to 1.0.

A number of empirical and more physically-based approaches exist to estimate atmospheric longwave emissivity from standard meteorological data (see Hock, 2005 for a discussion). For clear sky

325 conditions, Brutsaert (1975) developed a theoretically-based formula depending on air temperature and vapour pressure measured at screen level:

$$\varepsilon_{ac} = 1.24 \left( \frac{p_v}{T_a} \right)^{\frac{1}{7}} \quad (22)$$

where  $\varepsilon_{ac}$  is the clear sky longwave emissivity (–),  $p_v$  the actual vapour pressure (hPa), and  $T_a$  the air temperature (K). Later, Brutsaert reconciled eq. (22) with an empirical approach proposed by Swinbank, (1963)

$$\varepsilon_{ac} = 9.2 \times 10^{-6} T_a^2 \quad (23)$$

330 that considers the strong correlation between vapour pressure and air temperature, thus only air temperature is needed as input variable. Using the above relation, at an air temperature of 10 °C the atmospheric longwave radiation flux into the snowpack amounts to  $Q_{L,in} = 281 \text{ W m}^{-2}$  under clear sky conditions, which is less than the outgoing flux of  $310 \text{ W m}^{-2}$ , i.e. the snowpack will lose energy in this situation.

335 The variability of atmospheric emissivity due to cloud cover, which increases the longwave emissivity, is significantly higher than variations under clear sky conditions. Monteith and Unsworth (2013) give the simple linear relationship.

$$\varepsilon_a = (1 - 0.84c)\varepsilon_{ac} + 0.84c \quad (24)$$

where  $\varepsilon_a$  is the atmospheric longwave emissivity,  $c$  the fraction of cloud cover (–), and  $\varepsilon_{ac}$  is calculated by eq. (22) or eq. (23). For overcast conditions and an air temperature of 10 °C, eq. (24) yields an atmospheric emissivity of 0.96, which results in an atmospheric longwave radiation flux of  $Q_{L,in} = 351 \text{ W m}^{-2}$  and thus a positive flux of  $Q_L = 41 \text{ W m}^{-2}$  into the snowpack.

345 Although cloud cover is difficult to parameterise, as clouds can be highly variable in space and time and their effects on radiation depend on the different cloud genera, a strong correlation between cloud cover and sunshine duration is obvious. Doorenbos and Pruitt (1977) give a tabulated relation between cloudiness  $c$  and relative sunshine hours  $n/N$  (see eq. (11)), that can be fitted by the quadratic regression

$$c = 1 - 0.5544 \frac{n}{N} - 0.5483 \left( \frac{n}{N} \right)^2 \quad (25)$$

Nevertheless, in simple sky models usually a linear relation between cloudiness and relative sunshine hours is applied as a first approximation (e.g. Brutsaert, 1982; Annandale et al., 2002; Pelkowski, 2009) which, as Badescu and Paulescu (2011) showed by using probability distributions to develop relations between cloudiness and relative sunshine hours, is a first good estimate.

350 **3.2.3 Sensible Heat Exchange**

Sensible heat exchange describes the energy flux due to temperature differences between the air and the snow surface while air is permanently exchanged by wind turbulences. A frequent approach to parameterise turbulent heat transfer is the aerodynamic method, that explicitly includes wind speed as a variable (Braithwaite et al., 1998; Lehning et al., 2002; Hock, 2005)

$$Q_H = \rho_a c_p C_H u (T_a - T_s) \quad (26)$$

355 where  $\rho_a$  is the air density ( $\text{kg m}^{-3}$ ),  $c_p$  the specific (isobaric) heat capacity of air ( $1006 \text{ J kg}^{-1} \text{ }^{\circ}\text{C}^{-1}$ ),  $C_H$  the exchange coefficient for sensible heat (–),  $u$  the mean wind speed ( $\text{m s}^{-1}$ ),  $T_a$  the air temperature ( $^{\circ}\text{C}$ ), and  $T_s$  the temperature at the snow surface ( $^{\circ}\text{C}$ ).

The density of air  $\rho_a$  is a function of atmospheric pressure, air temperature, and humidity

$$\rho_a = \frac{M_d [p - (1 - e)p_v]}{RT_a} \quad (27)$$

360 where  $p$  is the atmospheric pressure (Pa),  $p_v$  the vapour pressure (Pa) (see eq. (32)),  $T_a$  the air temperature (K),  $M_d$  the molar mass of dry air ( $0.02897 \text{ kg mol}^{-1}$ ),  $R$  the universal gas constant ( $8.31446 \text{ J mol}^{-1} \text{ K}^{-1}$ ) and  $e$  the ratio of molar weights of water and dry air = 0.622. At usual air temperatures humidity has only a minor effect on the air density.

The decrease of atmospheric pressure with altitude  $z$  (m a.s.l.) can be estimated by the isothermal barometric formula

$$p(z) = p_0 \exp\left(-\frac{g M_d}{RT_a} z\right) \quad (28)$$

365 where  $p_0$  is the atmospheric pressure at sea level (Pa) and  $g$  the gravitational acceleration ( $\text{m s}^{-2}$ ). At an air temperature of  $0 \text{ }^{\circ}\text{C}$  and a standard atmospheric pressure at sea level of  $101.325 \text{ kPa}$ , the air density is  $1.29 \text{ kg m}^{-3}$  while e.g., at an altitude of  $2000 \text{ m a.s.l.}$  the atmospheric pressure reduces to  $78.9 \text{ kPa}$  and the air density becomes  $1.01 \text{ kg m}^{-3}$ .

The exchange coefficient  $C_H$  can be approximated with (Campbell and Norman, 1998)

$$C_H = \frac{k^2}{\ln\left(\frac{z_u}{z_m}\right) \ln\left(\frac{z_T}{z_h}\right)} \quad (29)$$

370 where  $k$  is the von Kármán's constant 0.41 (–),  $z_u$  and  $z_T$  the height of wind and temperature observation above the snow surface (m),  $z_m$  the momentum roughness parameter, and  $z_h$  the heat roughness parameter. For a snow surface, the roughness parameters are given by Walter et al., (2005) as  $z_m \sim 0.001 \text{ m}$  and  $z_h \sim 0.0002 \text{ m}$ .

As it can be seen from eq. (26), the sensible heat component depends mainly on wind speed and 375 temperature. During stable clear weather periods with typically light winds, the turbulent exchange is smaller on average than the radiation components. For example, a wind speed of  $1 \text{ m s}^{-1}$  and an air temperature of  $5 \text{ }^{\circ}\text{C}$  will result in a sensible heat flux of about  $15.5 \text{ W m}^{-2}$ . However, at warm rain events or at Föhn conditions with strong warm winds, turbulent exchange can significantly contribute to the melting process. For example, a Föhn event of 14 hours duration on 8<sup>th</sup> December 2006 at Altdorf 380 (Switzerland, 440 m a.s.l.) with an average air temperature of about  $16 \text{ }^{\circ}\text{C}$ , average relative humidity of 37% and average wind speed of  $14.6 \text{ m s}^{-1}$  resulted in a mean sensible heat flux of about  $700 \text{ W m}^{-2}$  during that duration.

### 3.2.4 Latent Energy of Condensation or Vapourisation

The latent energy exchange reflects the phase change of water vapour at the snow surface, either by 385 condensation of vapour contained in the air or by vapourisation of snow. Thus, it can either warm or cool the snowpack (Harpold and Brooks, 2018). The energy flux is dependent on the vapour gradient between the air and the snow surface and is, like the sensible heat exchange, a turbulent process that increases with the wind speed. Thus, the aerodynamic formulation is analogously to eq. (26)

$$Q_E = \rho_a \lambda_v C_E u (q_a - q_s) \quad (30)$$

where  $\lambda_v$  is the latent heat of vapourisation of water at  $0\text{ }^{\circ}\text{C}$  ( $2.501 \times 10^6 \text{ J kg}^{-1}$ ),  $C_E$  the exchange coefficient 390 for latent heat (-) which is assumed to be equal to the exchange coefficient for sensible heat  $C_H$ ,  $q_a$  the specific humidity of the air (-), and  $q_s$  the specific humidity at the snow surface (-).

The specific humidity  $q_a$  can be derived from measurements of relative humidity or dew point temperature. In cases where such data is not available, Walter et al., (2005) approximate the dew point 395 temperature by the minimum daily temperature. For any air temperature  $T$  ( $^{\circ}\text{C}$ ), the saturation vapour pressure  $p_s$  (Pa) can be calculated by an empirical expression known as the Magnus-Tetens equation in the general form (Lawrence, 2005)

$$p_s = C e^{\frac{A T}{B + T}} \quad (31)$$

where  $A$ ,  $B$ , and  $C$  are coefficients e.g. after Allen et al., (1998)  $A = 17.2694$ ,  $B = 237.3 \text{ }^{\circ}\text{C}$ ,  $C = 610.78 \text{ Pa}$ . At the snow surface, according to Lehning et al., (2002) the air temperature can be assumed equal to the snow surface temperature and eq. (31) is applied with coefficients for saturation vapour pressure over ice  $A = 21.8746$ ,  $B = 265.5 \text{ }^{\circ}\text{C}$ ,  $C = 610.78 \text{ Pa}$  (Murray, 1967). At a temperature of  $0\text{ }^{\circ}\text{C}$ , both coefficient sets yield the same saturation vapour pressure of  $p_s = 611 \text{ Pa}$ .

Knowing the relative humidity  $\psi$  (-) and the saturation vapour pressure  $p_s$  at a given air temperature, the actual vapour pressure  $p_v$  (Pa) can be calculated through the relation

$$p_v = \psi p_s \quad (32)$$

and subsequently the respective specific humidity by

$$q = \frac{e p_v}{p - (1 - e)p_v} \approx \frac{e}{p} p_v \quad (33)$$

405 with  $p$  the atmospheric pressure (Pa) and  $e$  the ratio of molar weights of water and dry air = 0.622 as in eq. (27). Assuming melting conditions with a snow temperature  $T_s = 0$  °C and saturated vapour conditions, the vapour pressure at the snow surface is  $p_{v,snow} = p_s(0$  °C) = 611 Pa. While at positive air temperatures the sensible heat flux is always warming the snowpack, the latent heat flux can cool the snow by vapourisation if the relative humidity of the air is low. Even when assuming a relative humidity 410 of 100%, the latent heat flux into the snowpack will be comparatively small if wind speed is low, e.g., about 13 W m<sup>-2</sup> at an air temperature of 5 °C and a wind speed of 1 m s<sup>-1</sup>.

### 3.2.5 Precipitation Heat

The heat transfer into the snowpack by lowering rain's temperature, that is usually assumed to be equal to the air temperature  $T_a$  (°C), down to the freezing point at 0°C can be estimated as

$$Q_P = c_w P T_a \quad (34)$$

415 where  $c_w$  is the specific heat capacity of water (4.2 kJ kg<sup>-1</sup> °C<sup>-1</sup>) and  $P$  is the daily rainfall depth (kg m<sup>-2</sup> d<sup>-1</sup>). The energy input from precipitation is usually quite small and even during extreme weather conditions, like heavy warm rain storms with temperatures of 15°C and a precipitation depth of 50 mm, that may occur e.g. during early winter in the alps, the mean daily energy flux from rain would be a moderate 36.5 W m<sup>-2</sup>.

### 420 3.2.6 Change in Internal Energy

The rate of change in the energy stored in the snowpack  $\Delta Q$  (W m<sup>-2</sup>) represents the internal energy gains and losses due to changes in the snowpack's temperature profile and due to phase changes, i.e., melting of the ice portion or refreezing of liquid water in the snowpack. Until the snowpack temperature is 425 isothermal at 0 °C, any melt produced in the surface layer that exceeds the liquid water holding capacity of the porous snow matrix will percolate downward and will be captured and refrozen in colder lower layers. This internal mass and energy transport process absorbs at least parts of the incoming energy, which reduces the energy available for melt and will thus reduce the actual *DDF*.

Under data-scarce conditions and particularly when only daily data is available, it is difficult to properly 430 quantify the change in the internal energy of the snowpack (see discussion in Sec. 5.2.1). Therefore, In our study we focus on melt periods when the snowpack is 'ripe', i.e. when the snowpack temperature is isothermal at 0 °C and the residual volumetric water content of about 8% (Lehning et al., 2002) is filled with liquid water. This assumption is not a limitation when analysing the contribution of each individual

energy flux component towards a resulting *DDF* as presented in following sections, but the additional energy needed for ‘warming’ the snowpack has to be taken into account when estimating the total *DDF* if a snowpack is not ‘ripe’ (see Figure 11).

#### 4. Results

In this section, the contribution of each energy-flux component  $Q_i$  to the lumped daily *DDF* is presented. For this purpose, the respective melt depth  $M_i$  is calculated according to eq. (3) and further converted into the corresponding degree-day factor component  $DDF_i$  using eq. (2). For the following exemplary calculations, the air temperature is assumed to stay always above 0 °C, thus degree-days  $T_{DD}$  (°C d) in eq. (2) have the same numerical value as the daily average air temperature  $T_a$  (°C) used in the calculation of several energy flux components.

Besides demonstrating the dependency of the *DDF* components on decisive parameters of the energy flux components, the presented tables in supplementary materials <sup>2</sup> and graphs in this section, which are based on the relationships given in section 3, can be used to estimate the *DDF* component values in case either observed data is not available or not sufficient for more sophisticated approaches. It should be noted that parameters are normalised where applicable, i.e., set to hypothetical values like clearness index  $K_T = 1$  or wind speed  $u = 1.0 \text{ m s}^{-1}$ , thus final *DDF* values can be obtained by multiplying the given figures by the actual values of those parameters. Furthermore, all results are based on the assumption that the snowpack is isothermal at 0 °C and in fully ripe state.

##### 4.1 Shortwave radiation component - *DDFs*

Shortwave radiation induced melt is usually considered the largest *DDF* component, especially at higher elevations as well as under dry climates. The net energy flux  $Q_s$  is calculated using eq. (5), which consists of three factors (a) latitude, (b) albedo, and (c) clearness index  $K_T$ . The dependency of *DDFs* on these factors is demonstrated in Figure 5 for the period between winter solstice (21<sup>st</sup> December) and summer solstice (21<sup>st</sup> June). As shortwave radiation is independent of air temperature and hence of degree-days, the corresponding melt is divided by a hypothetical degree-day value of 1 °C d to arrive at the presented *DDFs* values. In case of actually higher degree-days, the given *DDFs* values have to be divided accordingly.

Figure 5 (a) shows the variation of *DDFs* depending on latitude for the range 30° – 60° North, while albedo ( $A = 0$ ) and clearness index ( $K_T = 1$ ) are set constant. Obviously, there is a significant difference in *DDFs* for different latitudes around the winter solstice due to solar inclination, making latitude the predominant factor for *DDFs* at this time of the year. However, around the summer solstice, *DDFs* has nearly the same value at different latitudes because the lower solar angle at higher latitudes is

---

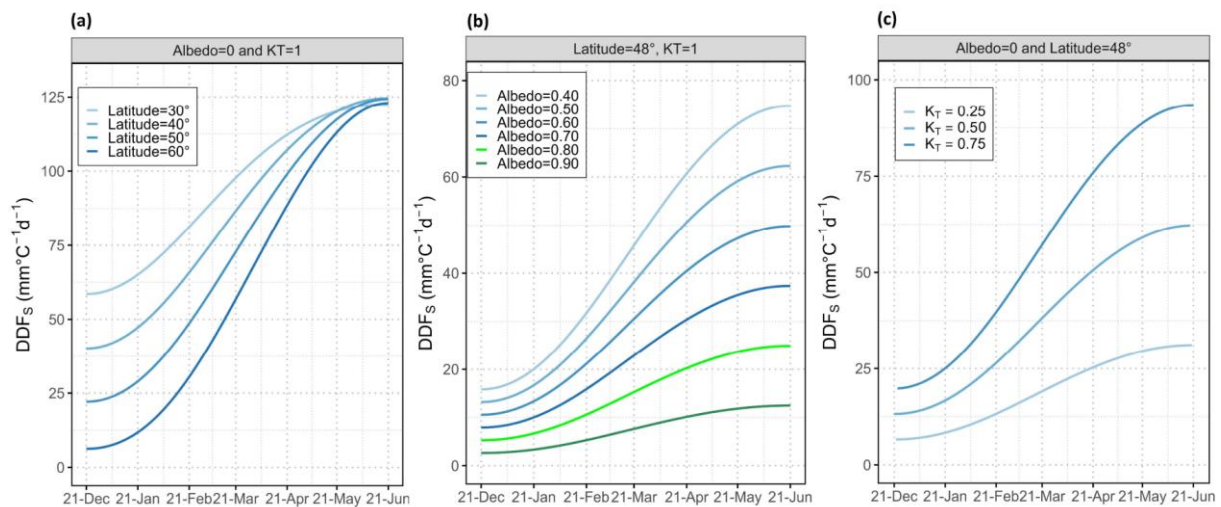
<sup>2</sup> S in numbering of Figures and Tables means that they are in Supplementary materials.

465 counterweighted by a larger hour angle, i.e., longer sunlight hours. Thus, with the progress of the melting season the factors albedo and clearness index become more important than latitude.

Figure 5 (b) shows the influence of albedo on the DDF<sub>S</sub> at a given latitude (Brunnenkopfhütte test site – latitude 48°) and normalised constant clearness index ( $K_T = 1$ ). Snow albedo varies between 0.9 – 0.4 covering the range between fresh and well-aged snow. As expected, the influence of albedo increases 470 with increasing incoming solar radiation towards the summer solstice. A good estimate of albedo is therefore much more important when the snowmelt season progresses than in early spring. If for example the same degree-day value of 10 °C d is assumed on 21<sup>st</sup> March and on 21<sup>st</sup> May, the difference in DDF<sub>S</sub> between fresh ( $A = 0.9$ ) and aged ( $A = 0.4$ ) snow would be 0.8 and 4.6 mm °C<sup>-1</sup> d<sup>-1</sup> in March compared to 1.2 and 7.1 mm °C<sup>-1</sup> d<sup>-1</sup> in May, respectively.

475 The dependency of DDF<sub>S</sub> on the clearness index  $K_T$  is shown in Figure 5 (c). In line with eq. (6), DDF<sub>S</sub> under clear sky ( $K_T = 0.75$ ) are always higher than under overcast conditions ( $K_T = 0.25$ ). Similar to albedo, the influence of the clearness index becomes more pronounced, with increasing solar angle when the snowmelt season progresses.

480 The influence of altitude on DDF<sub>S</sub> in terms of increasing  $K_T$  values can be assessed by multiplying a clearness index  $K_{T_0}$  at sea level, which may be obtained by any of the numerous solar radiation models, with a clearness altitude factor  $K_z$  (see eq. (18)). Figure 4 shows the range of clearness altitude factors for latitude 45° derived from eq. (14) – (17). All  $K_z$  values show a linear increase with altitude, with the slope depending on cloudiness. It should be noted that although the increase of  $K_z$  relative to  $K_{T_0}$  is 485 higher under overcast than under clear-sky conditions, the absolute increase of the clearness index  $K_T$  with altitude is larger for clear sky conditions (see Sec. 3.2.1). When using the intersection of all models and sky conditions, which is indicated by the dark grey area in Figure 4, in order to get one overall rough estimate of  $K_z$  for all conditions, the clearness altitude factor and thus the resulting DDF<sub>S</sub> is found to increase by about 6.4% per each 1000 m of altitude.



490

Figure 5 Variation of solar radiation based DDFs for a degree-day value of  $1^{\circ}\text{C d}$  for (a) different latitudes under constant snow albedo and clearness index; (b) snow albedos under constant latitude and clearness index; (c) different clearness indices under constant latitude and snow albedo – The latitude =  $48^{\circ}$  corresponds to the location of Brunnenkopfhütte test site.

495 **4.2 Longwave radiation component - DDF<sub>L</sub>**

The net longwave energy flux  $Q_L$  is calculated using eq. (21), in which the outgoing radiation from the snowpack can be assumed to be constant. Thus, the contribution of the longwave radiation component DDF<sub>L</sub> is mainly dependent on the air temperature and the emissivity of the atmosphere (e.g., in particularly cloudiness conditions). Figure 6 and Table S1 present the DDF<sub>L</sub> as a function of degree-days  $T_{DD}$  and cloudiness. For a wide range of degree-days, especially in conjunction with low cloudiness, the outgoing longwave energy flux is higher than the incoming, resulting in a theoretically negative degree-day factor that will reduce the total DDF. This means that the DDF<sub>L</sub> component under clear sky conditions is usually contributing to a cooling of the snowpack rather than to melting. Under overcast conditions, the DDF<sub>L</sub> is relatively constant around  $1 \text{ mm } ^{\circ}\text{C}^{-1} \text{ d}^{-1}$  with a maximum value of  $1.3 \text{ mm } ^{\circ}\text{C}^{-1} \text{ d}^{-1}$  at  $T_{DD} = 20^{\circ}\text{C d}$ . Although this contribution to the total DDF is small compared to the shortwave radiation component DDFs, it can be of importance at the onset of snowmelt in early spring, when the solar radiation is still low, and the albedo of fresh snow is high.

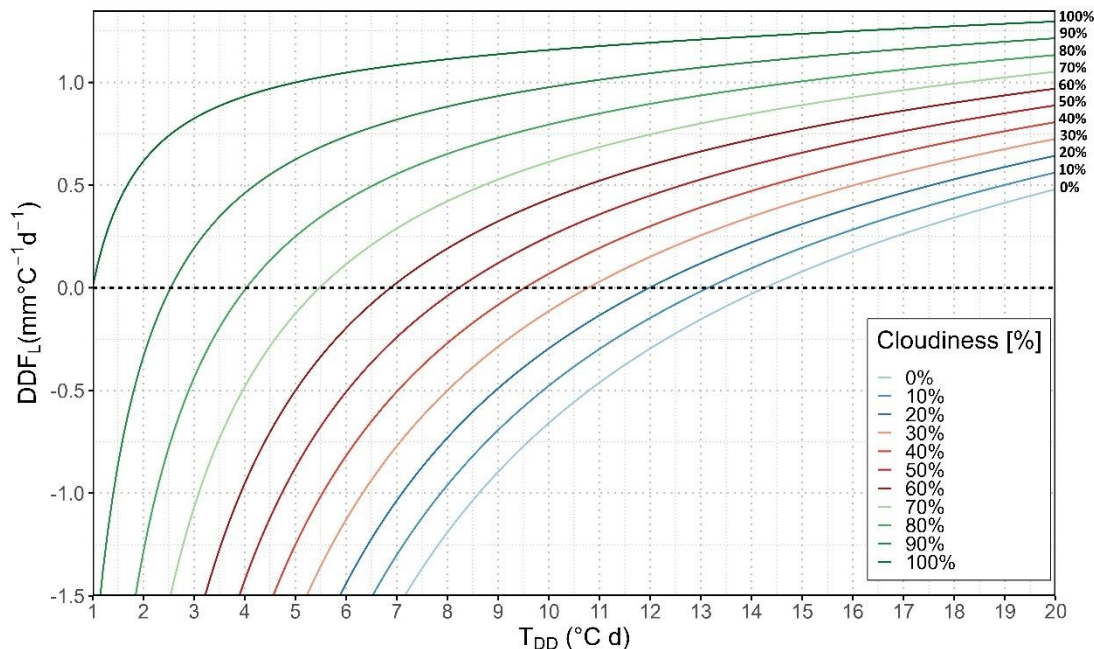


Figure 6 Longwave Radiation component (DDF<sub>L</sub>) for selected cloudiness (%) and degree-days ( $^{\circ}\text{C d}$ )

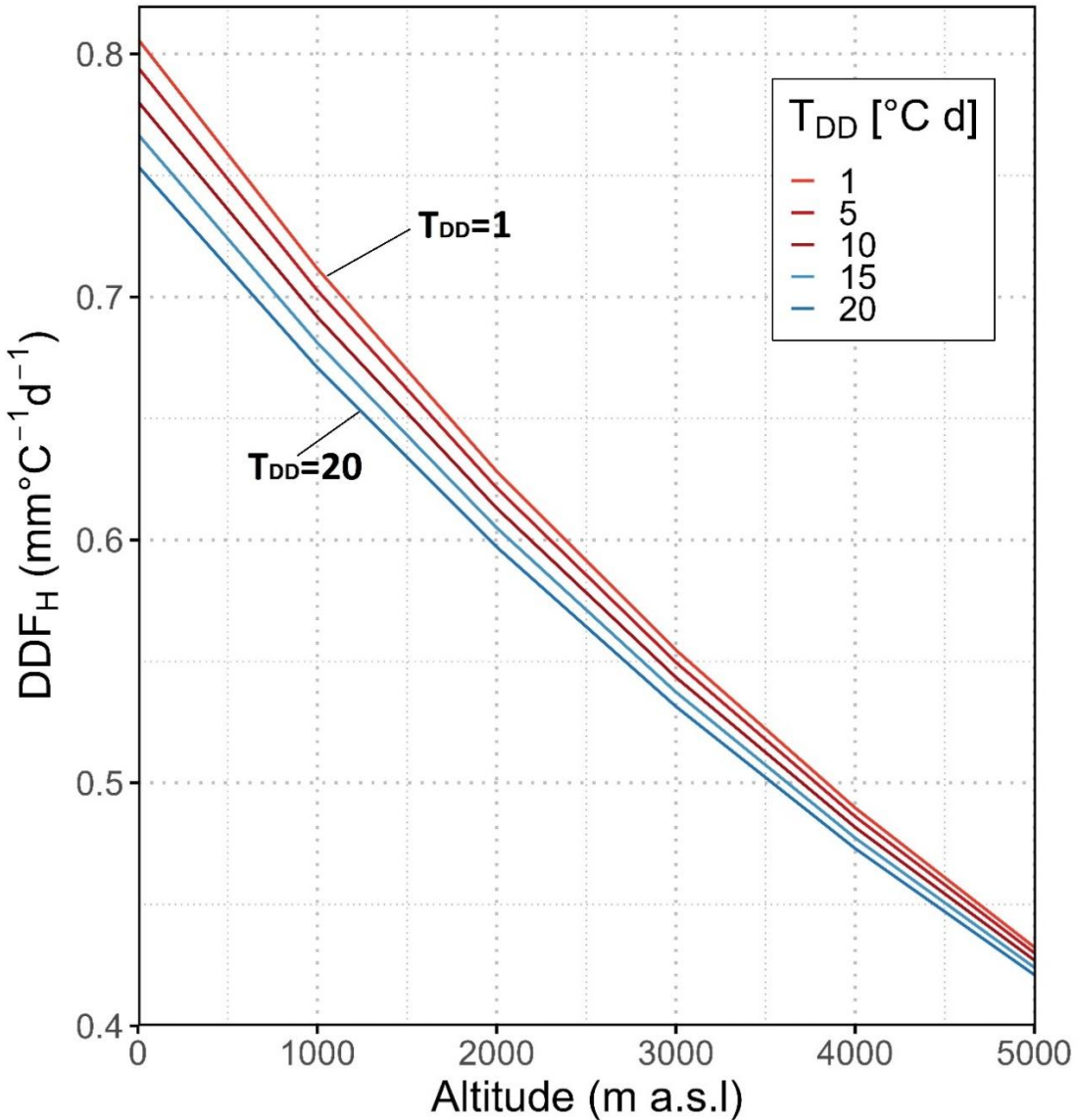
510 **4.3 Sensible heat component - DDF<sub>H</sub>**

The sensible heat flux  $Q_H$  as given by eq. (26) is mainly proportional to wind speed and the temperature difference between the air and the snow surface. Furthermore, air density, besides its dependency on temperature, is a function of relative humidity and atmospheric pressure, and thus of altitude (eq. (27)

and (28)). Since the influence of the relative humidity on air density is negligible, a relative humidity of 515  $RH = 0\%$  is assumed in the below analysis on the response of the  $DDF_H$  to changes in temperature resp. degree-days, wind speed and altitude. It should be noted that this analysis assumes typical melt conditions with a snowpack temperature of  $T_s = 0\text{ }^{\circ}\text{C}$  and positive air temperature, whereas negative air temperature would lead to a negative sensible heat flux resulting in a cooling of the snowpack and a decrease of total  $DDF$ .

520 Figure 7 and Table S2 show the variation in  $DDF_H$  depending on altitude and degree-days, while the wind speed is assumed to be constant at  $u = 1\text{ m s}^{-1}$ . The latter allows the  $DDF_H$  to be easily calculated for any other wind speed by multiplying the given value by the actual wind speed. The  $DDF_H$  principally decreases with altitude, with less pronounced differences due to temperature at higher altitudes. However, the most important factor is the wind speed. For example, with a daily average wind speed of 525  $u = 1.0\text{ m s}^{-1}$  e.g., at sea level  $z = 0\text{ m a.s.l.}$ , the  $DDF_H$  only decreases from  $0.806$  to  $0.781\text{ mm }^{\circ}\text{C}^{-1}\text{ d}^{-1}$  when degree-days increase from  $1$  to  $10\text{ }^{\circ}\text{C d}$  (See Figure 7 and Table S2). In contrast, for a degree-day of  $1\text{ }^{\circ}\text{C d}$ , the  $DDF_H$  increases proportionally from  $0.806$  to  $8.061\text{ mm }^{\circ}\text{C}^{-1}\text{ d}^{-1}$  when wind speed increases from  $1$  to  $10\text{ m s}^{-1}$ . Thus, wind speed is a decisive variable when estimating the  $DDF_H$ .

530 If wind speed observations are not available, they may be roughly estimated based on the topographic and climate characteristics of the study area. However, average values may not represent the actual wind conditions and thus  $DDF_H$  on a certain day. While for example the geometric mean of observed daily wind speed at the Brunnenkopfhütte station is about  $0.8\text{ m s}^{-1}$  resulting in a  $DDF_H$  of approx.  $0.7\text{ mm }^{\circ}\text{C}^{-1}\text{ d}^{-1}$ , the maximum daily average wind speed is about  $4.5\text{ m s}^{-1}$  which increases  $DDF_H$  to approx.  $3.9\text{ mm }^{\circ}\text{C}^{-1}\text{ d}^{-1}$ .



535

**Figure 7** Variation of sensible heat component ( $DDF_H$ ) at different altitude based on different degree-days,  $RH = 0\%$  and  $u = 1 \text{ m s}^{-1}$

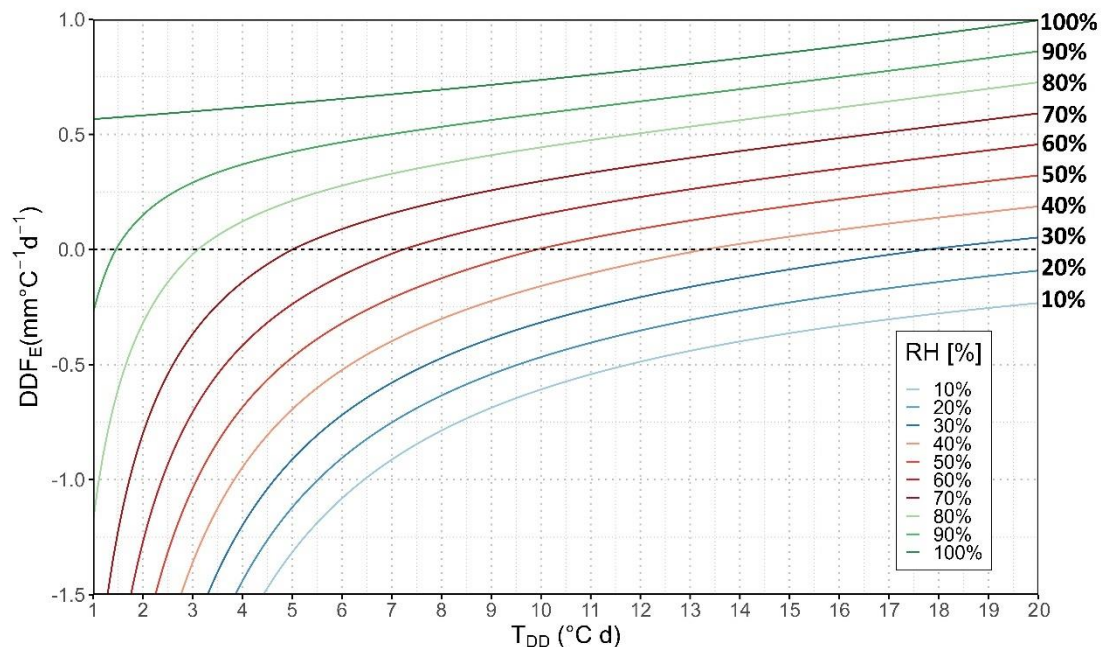
#### 4.4 Latent heat component - $DDF_E$

The latent heat flux  $Q_E$  approximated by an aerodynamic model as in eq. (30) indicates, that the latent heat component  $DDF_E$  is mainly dependent on the humidity gradient near the snow surface and on the wind speed. Additionally, altitude has an influence, as the air density is decreasing with altitude. Figure 8 and Table S3 give the resulting  $DDF_E$  as a function of degree-days for different values of relative humidity and at daily average wind of  $u = 1.0 \text{ m s}^{-1}$  whereas air density values are assumed at an elevation of 0 m a.s.l. In line with the sensible heat component  $DDF_H$ ,  $DDF_E$  for any other wind speed 540 can be obtained by multiplication by the actual value. For relative humidity  $< 30\%$  the  $DDF_E$  is negative 545

over the whole range of degree-days, hence the latent heat component will reduce the total  $DDF$  under these conditions. Even if the air is humid and warm, contribution of latent heat is moderate, e.g.,  $DDF_E = 1.0 \text{ mm } ^\circ\text{C}^{-1} \text{ d}^{-1}$  at a relative humidity of 100% and  $T_{DD} = 20 \text{ }^\circ\text{C d}$ .

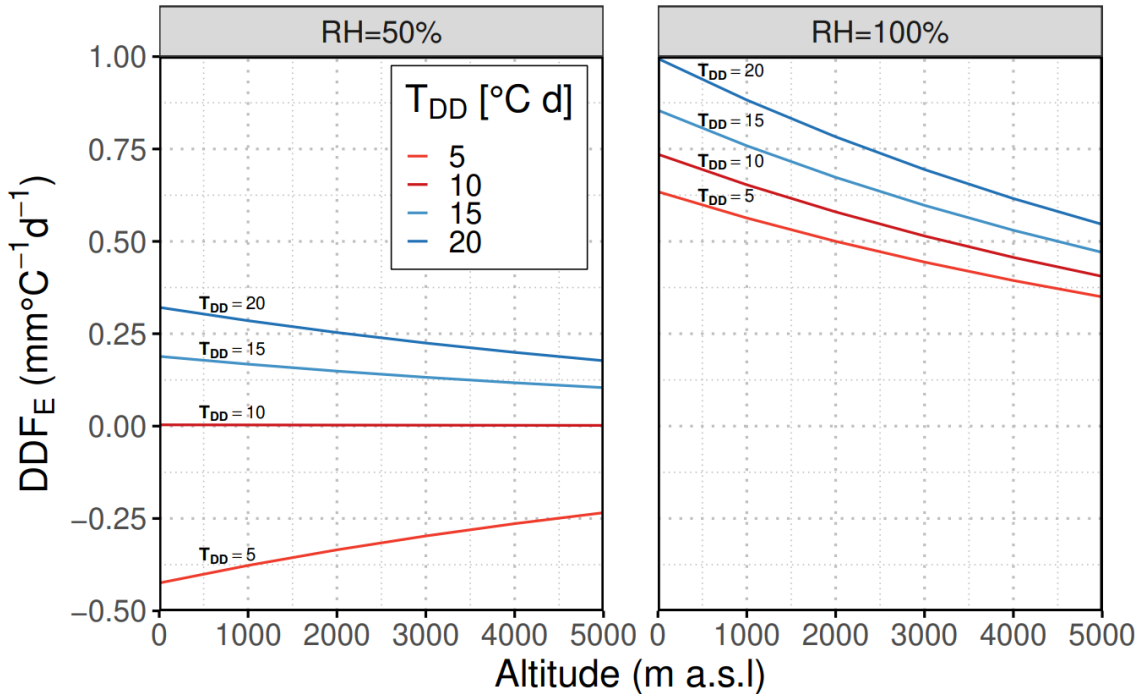
Figure 9 shows the combined effect of altitude, relative humidity, and temperature on  $DDF_E$ . At a high relative humidity (e.g.,  $RH = 100\%$ ), similar to the  $DDF_H$  the  $DDF_E$  values principally decrease with altitude, with less pronounced differences due to temperature at higher altitudes. At lower relative humidity (e.g.,  $RH = 50\%$ ), the altitude effect is less noticeable and at low temperatures even a reversal of the effect can be observed. Thus, altitude reduces positive  $DDF_E$  associated with high humidity while it also reduces the cooling effect of a negative latent heat flux, which is associated with low humidity and lower air temperature.

As the above analysis shows, humidity is the main variable influencing the  $DDF_E$ . In general, humid air will promote condensation at a cooler snow surface, which releases latent energy and contributes to a positive  $DDF$ , while dry air will promote evaporation and sublimation from the snow surface, which abstracts energy from the snowpack. Thus, mainly depending on the humidity of the air, the latent heat energy flux is usually a heat sink while only in case of high humidity in conjunction with higher temperature it becomes a heat source to the snowpack. Especially in spring, when relative humidity is comparatively low in middle and northern latitudes, large parts of the incoming solar radiation can be consumed by evaporation from the snow surface significantly reducing the energy available for melt and thus reducing the corresponding  $DDFs$  (Lang and Braun, 1990; Zhang et al., 2006).



565

**Figure 8** Latent Heat component ( $DDF_E$ ) for selected relative humidity (%), degree-days ( $^\circ\text{C d}$ ) and  $u = 1 \text{ (m s}^{-1}\text{)}$ , These values are for  $u = 1 \text{ m s}^{-1}$ , for a different wind speed these values can be multiplied for desired wind speed. Air density values are assumed at an elevation of 0 m a.s.l.



570 **Figure 9** Variation of latent heat component ( $DDF_E$ ) depending on altitude for different relative humidity values, degree-days and  $u=1 \text{ m s}^{-1}$

#### 4.5 Precipitation heat component – $DDF_P$

Rainfall can affect the snowpack energy budget by adding sensible heat due to warm rain and by releasing latent heat if the rain refreezes in the snowpack (DeWalle and Rango, 2008). The latter effect 575 is not considered in this study, as the snowpack is assumed at 0°C melting condition. Given that the precipitation heat  $Q_P$  is linearly dependent on air temperature in eq. (34), a division by respective degree-days makes  $DDF_P$  independent of temperature and proportional to rainfall, resulting in a  $DDF_P = 0.0125 \text{ mm } ^\circ\text{C}^{-1} \text{ d}^{-1}$  for a precipitation depth of 1 mm d<sup>-1</sup>.  $DDF_P$  for any other precipitation can be obtained by respective multiplication. The exemplary values in Table 2 show however, that the contribution of the 580 precipitation heat component  $DDF_P$  is modest compared to other  $DDF$  components. Even high rainfall of 50 mm d<sup>-1</sup> would release only a small amount of sensible heat, resulting in a  $DDF_P$  of 0.6 mm  $^\circ\text{C}^{-1} \text{ d}^{-1}$ .

**Table 2** Precipitation heat component ( $DDF_P$ ) ( $\text{mm } ^\circ\text{C}^{-1} \text{ d}^{-1}$ ) for selected precipitation ( $\text{mm d}^{-1}$ )

Precipitation ( $P$ )	1	2	5	10	25	50
$DDF_P$	0.0125	0.025	0.0625	0.125	0.313	0.625

#### 5. Discussion

585 While the previous section focuses on the characteristics of each individual energy flux based  $DDF$  component, this section mainly discusses the influence of spatial, seasonal or meteorological conditions on the overall  $DDF$ . The discussion section bifurcates into two sub-sections, (i) influence of individual factors on the  $DDF$  such as latitude, altitude, albedo, season and rain on snow events, and (ii) application

of energy-flux-based *DDF* estimates, discussing how this value can be estimated for a temperature-index model by using different available datasets and applied under varying meteorological and climate change conditions.

## 5.1 Influence of individual factors on the DDF

In this section all conclusions are under the assumption that the snowpack is isothermal at  $T_s = 0^\circ\text{C}$  and in ripe condition, hence all net incoming energy is available for melt and contributes to the total *DDF*.  
590 Apart from the discussed variables, we assumed with the following standard values  $u = 1 \text{ m s}^{-1}$ ,  $RH = 70\%$ ,  $A = 0.5$ ,  $P = 0 \text{ mm}$ , and typical melt conditions of  $T_{DD} = 5^\circ\text{C d}$  except if stated otherwise.

### 5.1.1 Influence of latitude

While topographic factors like slope, aspect or shading in mountainous regions result in a high local variability of melt conditions, larger scale regional patterns of *DDFs* (e.g., a dependency on latitude)  
600 could not be detected in a data review by Hock (2003). This observation is supported by a brief analysis of the effect of latitude below, where the *DDF* is compared not on the same date but at same degree-days. As an illustrative example, typical melt conditions of  $T_{DD} = 5^\circ\text{C d}$  at a latitude of about  $35^\circ$  North in the Upper Jhelum catchment (Bogacki and Ismail, 2016) are compared to similar conditions at a latitude of  $48^\circ$  North (Brunnenkopfhütte, 1602 m a.s.l.). As zone-wise temperature data (see Sec. 2.2)  
605 indicates, in the Upper Jhelum catchment at an elevation zone of 1500 – 2000 m a.s.l., melting conditions usually occur around mid-February while at Brunnenkopfhütte comparable degree-days are obtained about one month later in mid-March. Figure 10 (a) compares the energy flux based *DDF* components at both latitudes. The decisive solar radiation component is very similar at the two locations, both under clear sky and overcast conditions, thus the total *DDF* is virtually identical at both latitudes. Therefore,  
610 at least in moderate latitudes and when compared under similar melt conditions, no significant effect of latitude on *DDF* could be found.

### 5.1.2 Influence of altitude

Contrary to the compensating effect in the case of latitude, the delayed onset of snowmelt due to altitude influences the *DDF* noticeably, which becomes important in temperature-index models where  
615 calculation is usually based on elevation bands. In order to demonstrate the influence of altitude on the *DDF*, two elevation zones with an altitude of 1500 – 2000 and 3500 – 4000 m a.s.l., respectively, are compared at  $35^\circ$  latitude in the Upper Jhelum catchment. As indicated above, typical melt conditions of  $T_{DD} = 5^\circ\text{C d}$  occur at 1500 – 2000 m a.s.l. usually around mid-February, while at 3500 – 4000 m a.s.l.  
620 similar degree-days are obtained for mid-May. The resulting *DDFs* (see Figure 10 (b)) show a significant difference, both under clear sky and under overcast conditions, because of the different input in solar radiation caused by the alteration in solar angle between February and May. Figure 10 (b) shows an additional term  $DDF_A$  on top of the solar radiation component that represents the increase in incoming solar radiation due to the clearness altitude factor, which takes into account the increase of the clearness

index with altitude (see Sec. 3.2.1). Averaging the factors proposed by different solar radiation models (see Figure 4) results in an additional component  $DDF_A$  of 0.4 and  $1.4 \text{ mm } ^\circ\text{C}^{-1} \text{ d}^{-1}$  under clear sky and of 0.5 and  $1.6 \text{ mm } ^\circ\text{C}^{-1} \text{ d}^{-1}$  und overcast conditions at 1500 – 2000 and 3500 – 4000 m a.s.l., respectively.

While snow albedo is assumed constant at 0.5 in Figure 10 (b), taking into consideration the decrease of albedo as the snow ages (see Table 1, e.g.  $A = 0.74$  in February and  $A = 0.42$  in May) results in a more pronounced difference with altitude, i.e., a  $DDF$  of 0.3 compared to  $10.5 \text{ mm } ^\circ\text{C}^{-1} \text{ d}^{-1}$  under clear sky and of 2.7 versus  $7.3 \text{ mm } ^\circ\text{C}^{-1} \text{ d}^{-1}$  under overcast conditions for the two altitudes, respectively.

The increase of  $DDF$  with increasing altitude is in line with previous studies (e.g. (Hock, 2003; Kayastha and Kayastha, 2020)). For example, in the Nepalese Himalayan region, seasonal-average  $DDF$  increases from 7.7 to  $11.6 \text{ mm d}^{-1} ^\circ\text{C}^{-1}$  with respect to altitude ranging 4900 to 5300 m a.s.l. (Kayastha et al., 2000) whereas Kayastha and Kayastha, (2020) found that the model-calibrated range of the  $DDF$  in central Himalayan basin varies between  $7.0 - 9.0 \text{ mm d}^{-1} ^\circ\text{C}^{-1}$  over an approximate altitude range of 4000 – 8000 m a.s.l. As Kayastha et al., (2000) pointed out higher values of the  $DDF$  usually occur at very low temperatures since at higher altitudes the major driving factor to melt is the energy input by solar radiation.

### 5.1.3 Influence of albedo

As already discussed in the sections before, snow albedo is a critical parameter for the  $DDF$  since according to eq. (5) the albedo directly controls the net solar radiation flux into the snowpack. While albedo of fresh snow is well above 0.9, hence reflecting most of the incoming shortwave radiation, it drops rapidly when larger grains form due to snow metamorphism. Figure 10 (c) demonstrates the effect of aging snow after a new snow event, when a simple exponential decay model as given in eq. (19) is used and typical melting conditions  $T_{DD} = 5 \text{ } ^\circ\text{C d}$  are assumed. Since directly after a new snow event (Day = 0) the fresh snow albedo is high ( $A = 0.95$ ), the overall  $DDF$  is generally small. Under clear-sky conditions, in case longwave-radiation cooling is larger than net shortwave radiation flux, even a negative  $DDF$  value, i.e., no melt, may occur. If there is no new snow event in-between, albedo will decrease following the exponential decay model to 0.52 after 10 days resulting in a  $DDF$  of  $5.8 \text{ mm } ^\circ\text{C}^{-1} \text{ d}^{-1}$  under clear sky and  $4.4 \text{ mm } ^\circ\text{C}^{-1} \text{ d}^{-1}$  under overcast conditions. The increase in the  $DDF$  with exponential decay in albedo is in agreement with the findings of MacDougall et al., (2011), who found that the  $DDF$  is sensitive to albedo with values of  $> 4.0 \text{ mm d}^{-1} ^\circ\text{C}^{-1}$  at an albedo on 0.6. As described qualitatively in the literature e.g. (Hock, 2003), under all sky conditions the  $DDF$  is continuously increasing with decreasing albedo, with the increase however being more pronounced under clear-sky than under overcast conditions.

### 5.1.4 Influence of season

Since the solar angle is rising from its minimum at winter solstice in December to its maximum on 21<sup>st</sup> June, the solar radiation component  $DDF_S$  is increasing during the snowmelt season and thus the  $DDF$

is expected to increase respectively. Figure 10 (d) shows the influence of season on the *DDF* at the  
660 Brunnenkopfhütte test site during the melt period, assuming average degree-days of 1, 4, and 7 °C d in  
March, April, and May, respectively (see Table 1). Under clear-sky conditions, the total *DDF* increases  
from a negative value of  $-3.6 \text{ mm } ^\circ\text{C}^{-1} \text{ d}^{-1}$  in March to  $6.6 \text{ mm } ^\circ\text{C}^{-1} \text{ d}^{-1}$  in May. Under overcast conditions  
however, the *DDF* is virtually stable ranging from 4.4 to  $4.5 \text{ mm } ^\circ\text{C}^{-1} \text{ d}^{-1}$  in the same period. The stability  
665 of the *DDF* under overcast conditions found in our study is in agreement with the study of Kayastha et  
al. (2000), where the *DDFs* observed during July – August are small compared to June because of  
prevailing cloud cover due to monsoon activity, which reduces the incoming shortwave radiation.

An evaluation of the individual *DDF* components shows, that under clear-sky conditions the high impact  
of solar radiation in combination with low degree-days at the onset of the snowmelt season is  
counterweighted by a strong negative longwave radiation component that decreases as the season  
670 progresses. Under overcast conditions,  $\text{DDF}_L$  is neutral or slightly positive while the  $\text{DDF}_S$  component  
decreases because degree-days are rising faster than input from solar radiation, which implies that sky  
conditions (i.e., overcast, and clear sky) are more decisive for an estimate of the *DDF* than the day of  
the year.

The effect of cloud cover is further amplified by the decrease in albedo while the melt season progresses,  
675 which becomes more significant under clear sky conditions. In the present example (with the average  
monthly albedo as specified in Table 1) only 30% of incoming solar radiation is contributing to melt in  
March, while it is about 60% in May, enhancing the marked increase of the *DDF* under clear sky  
conditions.

### 5.1.5 Influence of rain on snow events

680 In general, the precipitation heat-component alone has only a minor effect on the *DDF*. However, in  
conjunction with certain weather conditions, like breaking in of warm and moist air, rain over snow  
events may lead to sudden melt and severe flooding.

Figure 10 (e) shows the different *DDF* components resulting from a hypothetical rain over snow event  
assuming an air temperature of 15 °C, a precipitation of  $70 \text{ mm d}^{-1}$ , a daily average wind speed of  $10 \text{ m}$   
685  $\text{s}^{-1}$ , a relative humidity of 100%, and overcast conditions. Although the amount of precipitation is  
substantial and the rain temperature is comparatively high, the contribution of  $\text{DDF}_P$  is still modest.  
However, air temperature, relative humidity, and in particular wind speed associated with such events  
increase the sensible and latent heat components significantly. Thus, the resulting overall *DDF* is much  
higher than under usual melt conditions, which may lead to a considerable melt that adds to the runoff  
690 already caused by the heavy rain.

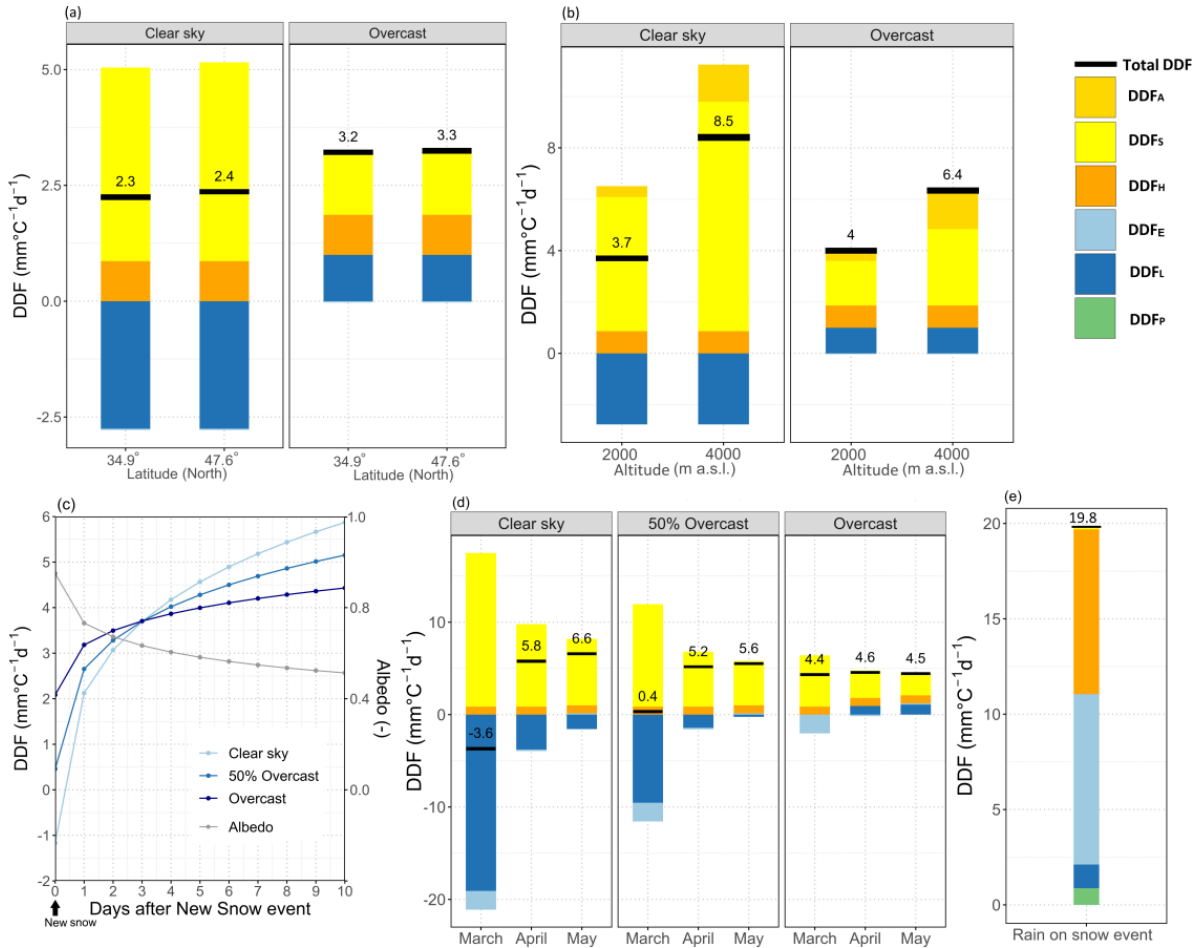


Figure 10 Influence of (a) latitude, (b) altitude, (c) albedo, (d) season, and (e) rain on snow events on the *DDF* under clear-sky and overcast conditions. *DDF* components: Shortwave radiation ( $DDF_S$ ), Longwave radiation ( $DDF_L$ ), Sensible heat ( $DDF_H$ ), Latent heat ( $DDF_E$ ), Precipitation Heat ( $DDF_P$ ) and increase in short wave component due to increase of the clearness index with altitude ( $DDF_A$ )

695

## 5.2 Application of energy flux based DDF estimates

### 5.2.1 DDF estimates under field conditions

In addition to the analysis of the influence of individual factors on the *DDF*, the dataset from the 700 Brunnenkopfhütte test site is used to compare energy flux-based estimates with field-derived DDFs in order to demonstrate how naturally varying meteorological conditions during the melt season, and in particular the cold content of the snowpack, affect the accuracy of *DDF* estimates.

For this purpose, daily melt was estimated from the daily difference of observed snow water equivalent during melt periods (see Figure 3). Energy flux-based melt was calculated by the formulas given in Sec. 705 3 using observed daily data from the Brunnenkopfhütte automatic snow and weather station (e.g., air temperature, wind speed, etc., see Sec. 2.1) where applicable.

The daily degree-day sum is calculated from hourly air temperature data as proposed by Braithwaite and Hughes (2022). In general, operational degree-day models typically use constant degree-day factors for

710 a certain time period (e.g., 10-daily period). In this backdrop, both energy-flux based, and data-derived daily melt values were accumulated on a 10-daily basis and divided by the degree-days of the respective period. The 10-daily averaging procedure also smooths daily noise in the observed data, in particular inaccuracies in the determination of daily melt and unrealistic *DDFs* values because of daily temperature averages just above 0 °C.

715 The comparison between field-derived and estimated (energy flux based) *DDFs* (see Figure 11) yields a fair agreement with bias = 0.14 mm °C<sup>-1</sup> d<sup>-1</sup> between estimated and field-derived values, and Root Mean Square Error (RMSE) = 1.12 mm °C<sup>-1</sup> d<sup>-1</sup>. Noteworthy in Figure 11 are the “new snow events”, where the snowpack is no longer ‘ripe’ and a certain amount of the incoming energy is needed to bring the snowpack back to ripe state, thus does not contributing to melt. For these events all estimated *DDFs* considerably overestimate the field-derived ones and were thus excluded from the calculation of the

720 error metrics.

725 It is of interest to estimate *DDFs* also in cases where the snowpack is not ‘ripe’, e.g. because of new snow events or due to radiational cooling during clear cold nights. An approach to account for the snowpack’s energy deficit, i.e. the energy needed to bring the snowpack temperature isothermal at 0°C, is the concept of ‘cold content’ (Marks et al., 1999; Schaeefli and Huss, 2011). The cold content is usually either estimated as a function of meteorological parameters or calculated by keeping track of the residuals of the snowpack energy balance (Jennings et al., 2018). For the latter, the SNOWPACK model (Lehning et al., 2002) is an excellent tool, which provides a highly detailed simulation of the vertical mass, energy, and besides other state variables the snow temperature distribution inside a snowpack. However, SNOWPACK requires a considerable number of meteorological input variables and

730 preferably at least hourly observations, both of which are usually not available in the context where degree-day models are employed.

735 Especially suited for data scarce conditions, Walter et al., (2005) apply a lumped approach that accounts for the cold content by changing the (isothermal) snowpack temperature depending on the daily net energy flux. When the incoming energy flux is sufficient to raise the snow temperature to 0°C or when it is already at 0°C the day before, all additional available energy produces melt. This approach, which does not need any additional data, however, seems to significantly overestimate the snowpack temperature particularly in situations with negative energy fluxes at night but a positive daily net balance, as a comparison with SNOWPACK simulations using data from Brunnenkopfhütte shows (see Supplementary materials S.2). Therefore, an appropriate parametrisation of the cold content under

740 limited data availability that would enable satisfactory estimates of *DDFs* in situations when the snowpack is not completely ripe, remains subject to further research.

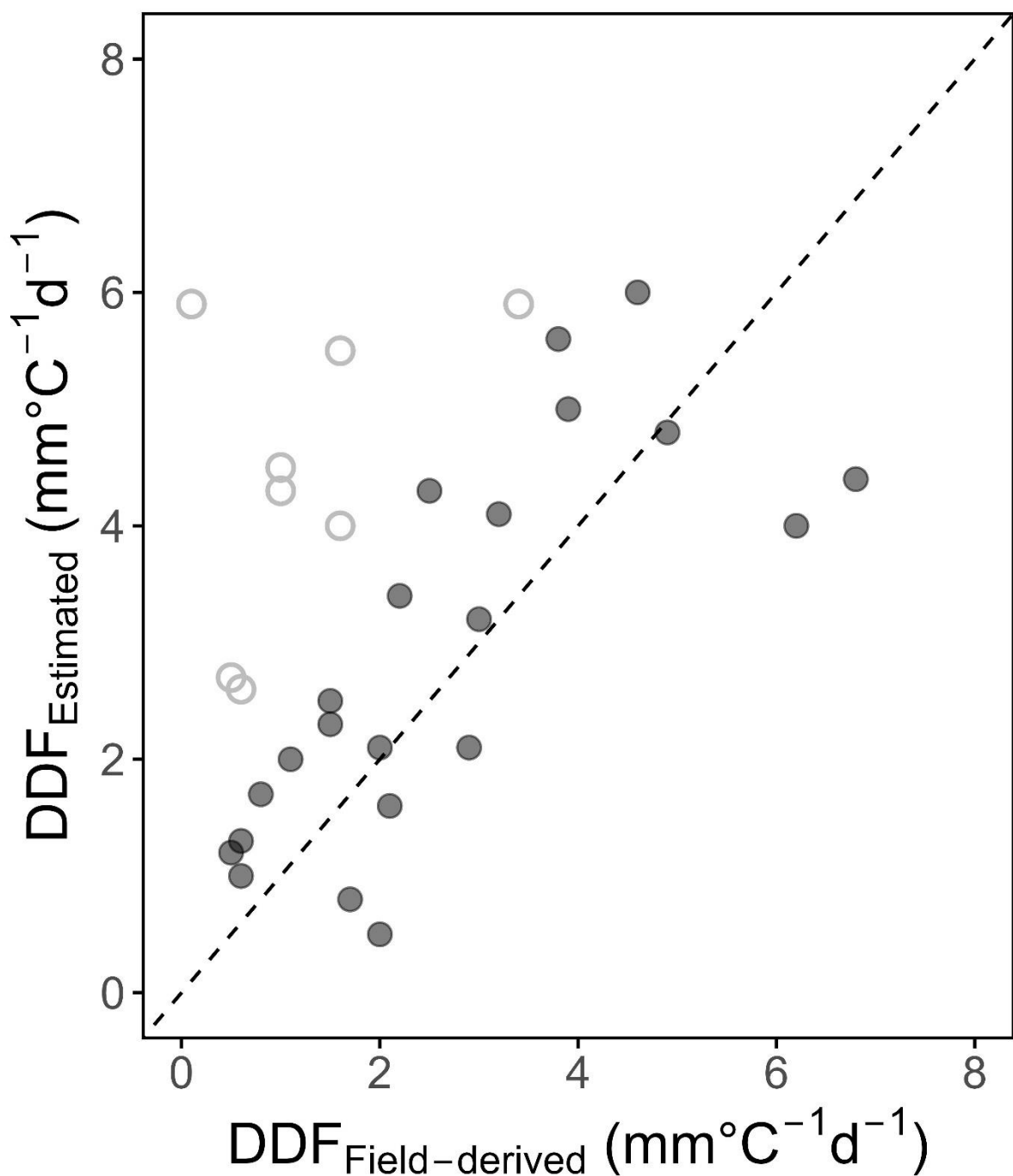


**Figure 11** Comparison of field-derived vs estimated (energy flux based) 10-daily DDF for the Brunnenkopfhütte test site (period: November 2016 – May 2021) – Hollow points represent DDFs during periods with new snow events (New snow: precipitation  $\geq 5 \text{ mm d}^{-1}$ )

## 5.2.2 DDF estimates for temperature-index modelling

Snowmelt runoff models using the temperature-index approach have proven to be useful tools for simulation and forecasting in large snow or glacier-dominated catchments, particularly in remote 750 mountainous regions where data is usually scarce. A good estimate of the degree-day factor as the decisive model parameter is important either to stay in a realistic range when calibrating this parameter or in case of forecasting when estimating its changes while the season progresses. In order to demonstrate the alteration of *DDFs* over time and altitude, energy-flux based *DDFs* are estimated using 10-daily average temperature (i.e. period 2000 – 2015) for the key elevation zones in the Upper Jhelum 755 catchment (Bogacki and Ismail, 2016). In the current example, the Upper Jhelum catchment is discussed because of elevation zone wise data availability in comparison to test site where only point data is available (for more detail see Sec. 2). Because of the lack of other than temperature and precipitation data, prevailing conditions during the melt season are crudely approximated by the standard conditions used in this section, assuming persistent clear sky conditions and albedo declining according to eq. (19) 760 after the last fresh snow event just before the beginning of the melting period.

Figure 12 shows the overall picture that how the *DDF* for snow will change over time and under climate change (i.e., Present, RCP2.6, RCP8.5 (for *DDF* estimates under climate change, see Sec. 5.2.3)). For example, Figure 12 (a) shows the development of *DDFs* in the elevation zones over time. As expected, melt starts earlier in lower elevation zones and successively progresses to higher altitudes. Interestingly, 765 the *DDF* in the first 10-daily period of melting in each elevation zone increases with altitude. This is a combined effect of (i) higher solar radiation input and decreasing albedo while the season progresses and the (ii) the onset of melt in higher elevation zones starting at a lower degree-day threshold than in lower zones. In contrast to Figure 10 (d), the *DDF* in Figure 12 decreases continuously in all elevation zones in the subsequent melting periods since air temperature and thus degree-days rise faster than melt. 770 The range of *DDFs* for snow estimated by the energy flux components is in good agreement with earlier studies for the Himalayan region, e.g.  $7.7 - 11.6 \text{ mm d}^{-1} \text{ }^{\circ}\text{C}^{-1}$  (Kayastha et al., 2000),  $5 - 9 \text{ mm d}^{-1} \text{ }^{\circ}\text{C}^{-1}$  (Zhang et al., 2006),  $5 - 7 \text{ mm d}^{-1} \text{ }^{\circ}\text{C}^{-1}$  (Tahir et al., 2011) and  $7.0 - 9.0 \text{ mm d}^{-1} \text{ }^{\circ}\text{C}^{-1}$  (Kayastha and Kayastha, 2020).

## 5.2.3 DDF estimates under the influence of climate change

775 Climate change will ultimately influence snowmelt patterns depending on the projected changes in temperature and precipitation. In recent studies, usually model parameters including *DDFs* are considered as constant when assessing the climate change impact on future water availability from snow and glacier fed catchments (Lutz et al., 2016; Hasson et al., 2019; Ismail et al., 2020). However, due to the physical processes on which they depend these parameters are subject to climate change. In this 780 section, an attempt is made to estimate the influence of climate change on the *DDFs* in different elevation zones. For this analysis, results from ISIMIP data (see Sec. 2.2), which predict the temperature

change for the period 2071 – 2100 to  $\Delta T = 2.3$  °C under RCP2.6 and  $\Delta T = 6.5$  °C under RCP8.5, are added to the temperatures in present climate for each elevation zone.

The first effect to be observed in Figure 12 (b) and (c) is the common finding that snowmelt will start earlier under climate change as temperatures rise earlier above freezing. In addition, since being earlier in the year, the *DDFs* in corresponding elevation zones are generally smaller compared to the current climate, though there are some outliers at the start of melting, due to division by low degree-day values. In case of the pessimistic RCP8.5 scenario (Figure 12 (c)), a seasonal snow cover will not establish anymore in the lowest elevation zone (i.e. 2500 – 3000 m a.s.l.) as air temperature at this elevation is projected to stay well above freezing throughout the winter. In general, the results of this brief analysis indicate, that the *DDFs* are expected to decrease under the influence of climate change, as the snowmelt season will shift earlier in the year when solar radiation is small and snow albedo values are expected to be on the higher side. Musselman et al., (2017), highlight similar findings about slower snowmelt in a warmer world due to a shift of the snowmelt season to a time of lower available energy. These results may contribute the important aspect to the recent discussion on the linearity of temperature-index models used for glacier mass balance predictions (Bolibar et al., 2022; Vincent and Thibert, 2022) that the key impact of climate change on the *DDF* is the shift in the melt season. This effect should be larger on snowmelt because the entire melt season will be shifted to a time with lower solar radiation, while the period of glacial melt in the present climate will be preserved and will only start earlier and last longer under climate change.

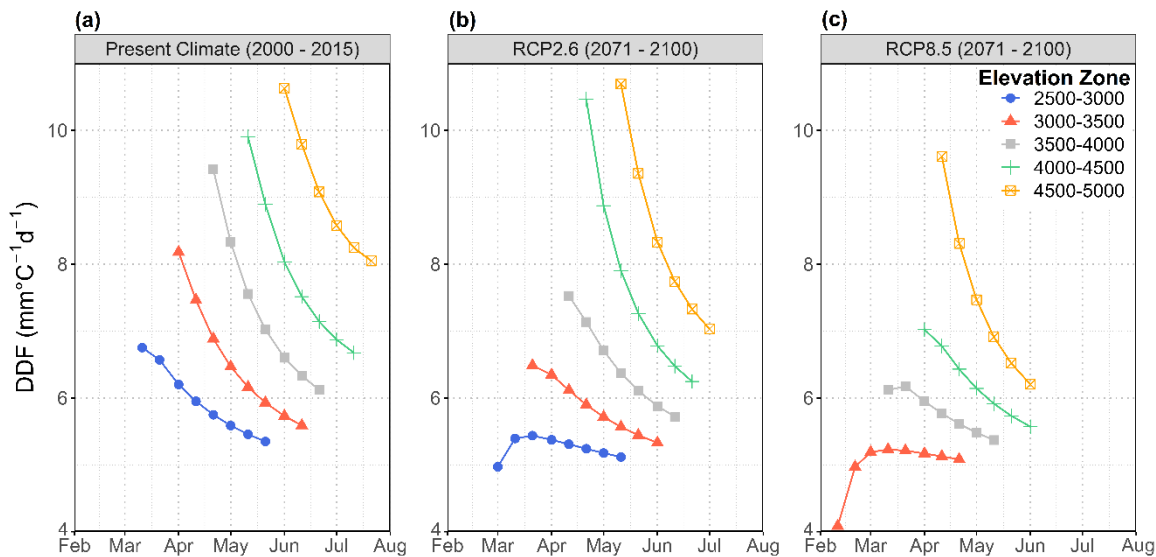


**Figure 12(a)** *DDF* estimates for a temperature-index modelling in present climate; (b) Influence of climate change – 2071 – 2100 under RCP2.6; (c) Influence of climate change – 2071 – 2100 under RCP8.5

## 805 6. Conclusions

Degree-day models are common and valuable tools for assessing present and future water availability in large snow- or glacier- melt dominated basins, in particular when data is scarce like e.g., in the

Hindukush-Karakoram-Himalayas Mountain ranges. The present study attempts to quantify the effects of spatial, temporal, and climatic conditions on the degree-day factor (*DDF*), in order to gain a better  
810 understanding of which influencing factors are decisive under which conditions. While this analysis is physically based on the energy balance, formulas with minimum data requirement for estimating the *DDFs* are used to account for situations where observed data is limited. In addition, resulting tables (see Supplementary materials S.1) and graphs for typical melt conditions are provided for a quick assessment.

A comparison between field-derived and estimated *DDFs* at the Brunnenkopfhütte test site shows a fair  
815 agreement with bias =  $0.14 \text{ mm } ^\circ\text{C}^{-1} \text{ d}^{-1}$  and RMSE =  $1.12 \text{ mm } ^\circ\text{C}^{-1} \text{ d}^{-1}$  over periods without new snow events, since fresh snow increases the cold content of the snowpack and contradicts the condition of the snowpack being ripe and isothermal at  $0 \text{ }^\circ\text{C}$ . Further research is needed for cases where under the constraint of limited data availability, also changes in the cold content of the snowpack are to be considered with a specific focus on approaches that parameterise the diurnal dynamics of vertical  
820 temperature distribution in the snowpack.

Furthermore, it is neither intended to use these *DDF* estimates directly as a model parameter nor to incorporate an energy-balance-based *DDF* approach into a degree-day model. One important aspect of temperature-index models is, that the *DDF* is a lumped parameter, which is usually subject to calibration and accounts for uncertainties in different variables and parameters, e.g., temperature estimates, runoff  
825 coefficients, etc. Thus, the *DDFs* estimated by the energy balance approach are rather aimed to validate the results of parameter calibration and to highlight necessary adjustments due to climate change.

The analysis of the energy-balance processes controlling snowmelt indicates that cloud cover is the most decisive factor for the dynamics of the *DDF*. Under overcast conditions, the contribution of shortwave radiation is comparatively low, whereas the other components are in general small. Therefore, total *DDF*  
830 value is not very high and variations due to other factors are usually limited, apart from exceptional rainstorm events, for which energy balance models are the more suitable approach.

Under clear-sky conditions on the other hand, shortwave radiation is the most prominent component contributing to melt. The increase of solar angle while the melt season progresses in combination with declining albedo and a decreasing cooling effect by the longwave radiation component along with  
835 increasing air temperature leads to a pronounced temporal dynamic in the *DDF*. Whereas incoming solar radiation and net longwave radiation can be determined fairly accurate by under clear-sky conditions, albedo becomes the crucial parameter for estimating the *DDF*, especially when new snow events occur during the melt period.

Clear-sky conditions promote the effect of increasing *DDF* with altitude if similar melting conditions  
840 are compared, since melting temperatures arrive later in the season at higher altitudes. The opposite effect can be observed with regard to climate change. Under higher temperatures at a given altitude, climate change will shift the snowmelt season earlier in the year. Consequently, when comparing periods

of similar degree-days, our study suggests *DDFs* are to decrease, since solar radiation is to generally decrease and albedo to typically increase.

845 Therefore, and as pointed out by many researchers, the *DDF* cannot be considered as a constant model parameter. Rather, its spatial and temporal variability must be taken into account, especially when using temperature-index models for forecasting present or predicting future snowpack and glacier changes, and the resulting water availability projections.

850

*Author contributions*

855 **MFI:** Conceptualization, Methodology, Software, Formal analysis, Investigation, Data curation, Writing – original draft, editing, Visualization. **WB:** Conceptualization, Methodology, Software, Formal analysis, Investigation, Data curation, Writing – reviewing & editing. **MD:** Supervision, review & editing. **MS:** Data curation, review & editing, **LK:** Supervision, Data curation.

*Competing Interest*

The contact author has declared that neither they nor their co-authors have any competing interests.

*Acknowledgements*

860 We would like to thank Technical University of Munich for funding the article. We also thank Koblenz University of Applied Sciences for funding the snow and meteorological station. We would like to thank all the reviewers and editor and in particular Roger Braithwaite for their valuable comments which helped to improve the manuscript considerably.

865

## 7. References

Ahmad, M. J. and Tiwari, G. N.: Solar radiation models-A review, *Int. J. Energy Res.*, 35, 271–290, <https://doi.org/10.1002/er.1690>, 2011.

Allen, R. G., Pereira, L. S., Raes, D., and Smith, M.: Crop evapotranspiration —guidelines for computing crop water requirements, FAO, 56, 1998.

Amaral, T., Wake, C. P., Dibb, J. E., Burakowski, E. A., and Stampone, M.: A simple model of snow albedo decay using observations from the Community Collaborative Rain, Hail, and Snow-Albedo (CoCoRaHS-Albedo) Network, *J. Glaciol.*, 63, 877–887, <https://doi.org/10.1017/jog.2017.54>, 2017.

Ambach, W.: Characteristics of the Heat Balance of the Greenland Ice sheet for Modelling, *J. Glaciol.*, 31, 3–12, <https://doi.org/10.3189/S0022143000004925>, 1985.

Anderson, E. A.: National Weather Service river forecast system: snow accumulation and ablation model, 1973.

Anderson, E. A.: Snow Accumulation and Ablation Model - SNOW-17, NOAA's National Weather Service, Office of Hydrologic Development, Silver Spring, 2006.

Annandale, J., Jovanovic, N., Benadé, N., and Allen, R.: Software for missing data error analysis of Penman-Monteith reference evapotranspiration, *Irrigation Science*, 21, 57–67, <https://doi.org/10.1007/s002710100047>, 2002.

Arendt, A. A. and Sharp, M. J.: Energy balance measurements on a Canadian high Arctic glacier and their implications for mass balance modelling, *IAHS-AISH publication*, 165–172, 1999.

Asaoka, Y. and Kominami, Y.: Incorporation of satellite-derived snow-cover area in spatial snowmelt modeling for a large area: determination of a gridded degree-day factor, *Ann. Glaciol.*, 54, 205–213, <https://doi.org/10.3189/2013AoG62A218>, 2013.

Badescu, V. (Ed.): Modeling solar radiation at the earth's surface: recent advances, Springer, Berlin, 517 pp., 2008.

Badescu, V. and Paulescu, M.: Statistical properties of the sunshine number illustrated with measurements from Timisoara (Romania), *Atmospheric Research*, 101, 194–204, <https://doi.org/10.1016/j.atmosres.2011.02.009>, 2011.

Bagchi, A. K.: Areal value of degree-day factor / Valeur spatiale du facteur degré-jour, *Hydrological Sciences Journal*, 28, 499–511, <https://doi.org/10.1080/0262668309491991>, 1983.

Bergström, S.: Development and application conceptual runoff model for scandinavian catchments, SMHI, Research Department, Hydrology, 162, 1976.

Bogacki, W. and Ismail, M. F.: Seasonal forecast of Kharif flows from Upper Jhelum catchment, *Proc. IAHS*, 374, 137–142, <https://doi.org/10.5194/piahs-374-137-2016>, 2016.

Bolibar, J., Rabatel, A., Gouttevin, I., Zekollari, H., and Galiez, C.: Nonlinear sensitivity of glacier mass balance to future climate change unveiled by deep learning, *Nat Commun*, 13, 409, <https://doi.org/10.1038/s41467-022-28033-0>, 2022.

Bormann, K. J., Evans, J. P., and McCabe, M. F.: Constraining snowmelt in a temperature-index model using simulated snow densities, *Journal of Hydrology*, 517, 652–667, <https://doi.org/10.1016/j.jhydrol.2014.05.073>, 2014.

Braithwaite, R. J.: Positive degree-day factors for ablation on the Greenland ice sheet studied by energy-balance modelling, *J. Glaciol.*, 41, 153–160, <https://doi.org/10.3189/S0022143000017846>, 1995.

Braithwaite, R. J.: Temperature and precipitation climate at the equilibrium-line altitude of glaciers expressed by the degree-day factor for melting snow, *J. Glaciol.*, 54, 437–444, <https://doi.org/10.3189/00221430878536968>, 2008.

Braithwaite, R. J. and Hughes, P. D.: Positive degree-day sums in the Alps: a direct link between glacier melt and international climate policy, *J. Glaciol.*, 1–11, <https://doi.org/10.1017/jog.2021.140>, 2022.

Braithwaite, R. J., Konzelmann, T., Marty, C., and Olesen, O. B.: Reconnaissance Study of glacier energy balance in North Greenland, 1993–94, *J. Glaciol.*, 44, 239–247, <https://doi.org/10.3189/S0022143000002586>, 1998.

Braun, L. N.: Simulation of snowmelt-runoff in lowland and lower alpine regions of Switzerland, Ph.D. Thesis, ETH Zurich, <https://doi.org/10.3929/ETHZ-A-000334295>, 1984.

Braun, Ludwig., Grabs, W., and Rana, B.: Application of a Conceptual Precipitation Runoff Model in the Langtang Kfaola Basin, Nepal Himalaya, *Snow and Glacier Hydrology*, 1993.

Bristow, K. L. and Campbell, G. S.: On the relationship between incoming solar radiation and daily maximum and minimum temperature, *Agricultural and Forest Meteorology*, 31, 159–166, [https://doi.org/10.1016/0168-1923\(84\)90017-0](https://doi.org/10.1016/0168-1923(84)90017-0), 1984.

Brutsaert, W.: On a derivable formula for long-wave radiation from clear skies, *Water Resour. Res.*, 11, 742–744, <https://doi.org/10.1029/WR011i005p00742>, 1975.

Brutsaert, W.: *Evaporation into the Atmosphere*, Springer Netherlands, Dordrecht, <https://doi.org/10.1007/978-94-017-1497-6>, 1982.

Campbell, G. S. and Norman, J. M.: *Introduction to environmental biophysics*, 2nd ed., Springer, New York, 286 pp., 1998.

Carenzo, M., Pellicciotti, F., Rimkus, S., and Burlando, P.: Assessing the transferability and robustness of an enhanced temperature-index glacier-melt model, *J. Glaciol.*, 55, 258–274, <https://doi.org/10.3189/002214309788608804>, 2009.

DeWalle, D. R. and Rango, A.: *Principles of Snow Hydrology*, Cambridge University Press, Cambridge, <https://doi.org/10.1017/CBO9780511535673>, 2008.

Doorenbos, J. and Pruitt, W. O.: Guidelines for predicting crop water requirements, Rev., Food and Agriculture Organization of the United Nations, Rome, 144 pp., 1977.

Ekici, C.: Total Global Solar Radiation Estimation Models and Applications: A review, *IJITIS*, 2, 212–228 Pages, <https://doi.org/10.15157/IJITIS.2019.2.2.212-228>, 2019.

Evrendilek, F. and Ertekin, C.: Assessing solar radiation models using multiple variables over Turkey, *Clim Dyn*, 31, 131–149, <https://doi.org/10.1007/s00382-007-0338-6>, 2008.

Frieler, K., Lange, S., Piontek, F., Reyer, C. P. O., Schewe, J., Warszawski, L., Zhao, F., Chini, L., Denvil, S., Emanuel, K., Geiger, T., Halladay, K., Hurt, G., Mengel, M., Murakami, D., Ostberg, S., Popp, A., Riva, R., Stevanovic, M., Suzuki, T., Volkholz, J., Burke, E., Ciais, P., Ebi, K., Eddy, T. D., Elliott, J., Galbraith, E., Gosling, S. N., Hattermann, F., Hickler, T., Hinkel, J., Hof, C., Huber, V., Jägermeyr, J., Krysanova, V., Marcé, R., Müller Schmied, H., Mouratiadou, I., Pierson, D., Tittensor, D. P., Vautard, R., van Vliet, M., Biber, M. F., Betts, R. A., Bodirsky, B. L., Deryng, D., Frolking, S., Jones, C. D., Lotze, H. K., Lotze-Campen, H., Sahajpal, R., Thonicke, K., Tian, H., and Yamagata, Y.: Assessing the impacts of 1.5 °C global warming – simulation protocol of the Inter-Sectoral Impact

Model Intercomparison Project (ISIMIP2b), Geosci. Model Dev., 10, 4321–4345, <https://doi.org/10.5194/gmd-10-4321-2017>, 2017.

Gafurov, A.: Water balance modeling using remote sensing information: focus on Central Asia, Ph.D. Thesis, Inst. f. Wasserbau, Stuttgart, 116 pp., 2010.

Hargreaves, G. H. and Samani, Z. A.: Estimating Potential Evapotranspiration, *J. Irrig. and Drain. Div.*, 108, 225–230, <https://doi.org/10.1061/JRCEA4.0001390>, 1982.

Harpold, A. A. and Brooks, P. D.: Humidity determines snowpack ablation under a warming climate, *Proc Natl Acad Sci USA*, 115, 1215–1220, <https://doi.org/10.1073/pnas.1716789115>, 2018.

Hasson, S. ul, Saeed, F., Böhner, J., and Schleussner, C.-F.: Water availability in Pakistan from Hindu Kush–Karakoram–Himalayan watersheds at 1.5 °C and 2 °C Paris Agreement targets, *Advances in Water Resources*, 131, 103365, <https://doi.org/10.1016/j.advwatres.2019.06.010>, 2019.

He, Z. H., Parajka, J., Tian, F. Q., and Blöschl, G.: Estimating degree-day factors from MODIS for snowmelt runoff modeling, *Hydrol. Earth Syst. Sci.*, 18, 4773–4789, <https://doi.org/10.5194/hess-18-4773-2014>, 2014.

Hempel, S., Frieler, K., Warszawski, L., Schewe, J., and Piontek, F.: A trend-preserving bias correction – the ISI-MIP approach, *Earth Syst. Dynam.*, 4, 219–236, <https://doi.org/10.5194/esd-4-219-2013>, 2013.

Hinzman, L. D. and Kane, D. L.: Snow hydrology of a headwater Arctic basin: 2. Conceptual analysis and computer modeling, *Water Resour. Res.*, 27, 1111–1121, <https://doi.org/10.1029/91WR00261>, 1991.

Hock, R.: A distributed temperature-index ice- and snowmelt model including potential direct solar radiation, *J. Glaciol.*, 45, 101–111, <https://doi.org/10.3189/S0022143000003087>, 1999.

Hock, R.: Temperature index melt modelling in mountain areas, *Journal of Hydrology*, 282, 104–115, [https://doi.org/10.1016/S0022-1694\(03\)00257-9](https://doi.org/10.1016/S0022-1694(03)00257-9), 2003.

Hock, R.: Glacier melt: a review of processes and their modelling, *Progress in Physical Geography: Earth and Environment*, 29, 362–391, <https://doi.org/10.1191/0309133305pp453ra>, 2005.

Hock, R. and Noetzli, C.: Areal melt and discharge modelling of Storglaciären, Sweden, *Ann. Glaciol.*, 24, 211–216, <https://doi.org/10.3189/S0260305500012192>, 1997.

Huss, M. and Hock, R.: Global-scale hydrological response to future glacier mass loss, *Nature Clim Change*, 8, 135–140, <https://doi.org/10.1038/s41558-017-0049-x>, 2018.

Immerzeel, W. W., Droogers, P., de Jong, S. M., and Bierkens, M. F. P.: Large-scale monitoring of snow cover and runoff simulation in Himalayan river basins using remote sensing, *Remote Sensing of Environment*, 113, 40–49, <https://doi.org/10.1016/j.rse.2008.08.010>, 2009.

Immerzeel, W. W., Lutz, A. F., Andrade, M., Bahl, A., Biemans, H., Bolch, T., Hyde, S., Brumby, S., Davies, B. J., Elmore, A. C., Emmer, A., Feng, M., Fernández, A., Haritashya, U., Kargel, J. S., Koppes, M., Kraaijenbrink, P. D. A., Kulkarni, A. V., Mayewski, P. A., Nepal, S., Pacheco, P., Painter, T. H., Pellicciotti, F., Rajaram, H., Rupper, S., Sinisalo, A., Shrestha, A. B., Vivioli, D., Wada, Y., Xiao, C., Yao, T., and Baillie, J. E. M.: Importance and vulnerability of the world's water towers, *Nature*, 577, 364–369, <https://doi.org/10.1038/s41586-019-1822-y>, 2020.

Ismail, M. F. and Bogacki, W.: Scenario approach for the seasonal forecast of Kharif flows from the Upper Indus Basin, *Hydrol. Earth Syst. Sci.*, 22, 1391–1409, <https://doi.org/10.5194/hess-22-1391-2018>, 2018.

Ismail, M. F., Bogacki, W., and Muhammad, N.: Degree-day factor models for forecasting the snowmelt runoff for Naran watershed, *SI*, 27, 1951–1960, 2015.

Ismail, M. F., Naz, B. S., Wortmann, M., Disse, M., Bowling, L. C., and Bogacki, W.: Comparison of two model calibration approaches and their influence on future projections under climate change in the Upper Indus Basin, *Climatic Change*, 163, 1227–1246, <https://doi.org/10.1007/s10584-020-02902-3>, 2020.

Jansson, P., Hock, R., and Schneider, T.: The concept of glacier storage: a review, *Journal of Hydrology*, 282, 116–129, [https://doi.org/10.1016/S0022-1694\(03\)00258-0](https://doi.org/10.1016/S0022-1694(03)00258-0), 2003.

Jennings, K. S., Kittel, T. G. F., and Molotch, N. P.: Observations and simulations of the seasonal evolution of snowpack cold content and its relation to snowmelt and the snowpack energy budget, *The Cryosphere*, 12, 1595–1614, <https://doi.org/10.5194/tc-12-1595-2018>, 2018.

Jin, Z., Yezheng, W., and Gang, Y.: General formula for estimation of monthly average daily global solar radiation in China, *Energy Conversion and Management*, 46, 257–268, <https://doi.org/10.1016/j.enconman.2004.02.020>, 2005.

Kane, D. L., Gieck, R. E., and Hinzman, L. D.: Snowmelt Modeling at Small Alaskan Arctic Watershed, *Journal of Hydrologic Engineering*, 2, 204–210, [https://doi.org/10.1061/\(ASCE\)1084-0699\(1997\)2:4\(204\)](https://doi.org/10.1061/(ASCE)1084-0699(1997)2:4(204)), 1997.

Kayastha, R. B. and Kayastha, R.: Glacio-Hydrological Degree-Day Model (GDM) Useful for the Himalayan River Basins, in: *Himalayan Weather and Climate and their Impact on the Environment*, edited by: Dimri, A. P., Bookhagen, B., Stoffel, M., and Yasunari, T., Springer International Publishing, Cham, 379–398, [https://doi.org/10.1007/978-3-030-29684-1\\_19](https://doi.org/10.1007/978-3-030-29684-1_19), 2020.

Kayastha, R. B., Ageta, Y., and Nakawo, M.: Positive degree-day factors for ablation on glaciers in the Nepalese Himalayas: case study on Glacier AX010 in Shorong Himal, Nepal, *Bulletin of glaciological research*, 1–10, 2000.

Kayastha, R. B., Yutaka, A., Masayoshi, N., Koji, F., Akiko, S., and Yoshihiro, M.: Positive degree-day factors for ice ablation on four glaciers in the Nepalese Himalayas and Qinghai-Tibetan Plateau, *Bulletin of glaciological research*, 7–14, 2003.

Klok, E. J., Jasper, K., Roelofsma, K. P., Gurtz, J., and Badoux, A.: Distributed hydrological modelling of a heavily glaciated Alpine river basin, *Hydrological Sciences Journal*, 46, 553–570, <https://doi.org/10.1080/02626660109492850>, 2001.

Kopp, G. and Lean, J. L.: A new, lower value of total solar irradiance: Evidence and climate significance: FRONTIER, *Geophys. Res. Lett.*, 38, n/a-n/a, <https://doi.org/10.1029/2010GL045777>, 2011.

Kopp, M., Tuo, Y., and Disse, M.: Fully automated snow depth measurements from time-lapse images applying a convolutional neural network, *Science of The Total Environment*, 697, 134213, <https://doi.org/10.1016/j.scitotenv.2019.134213>, 2019.

Kustas, W. P., Rango, A., and Uijlenhoet, R.: A simple energy budget algorithm for the snowmelt runoff model, *Water Resour. Res.*, 30, 1515–1527, <https://doi.org/10.1029/94WR00152>, 1994.

Lang, H.: Forecasting Meltwater Runoff from Snow-Covered Areas and from Glacier Basins, in: *River Flow Modelling and Forecasting*, vol. 3, edited by: Kraijenhoff, D. A. and Moll, J. R., Springer Netherlands, Dordrecht, 99–127, [https://doi.org/10.1007/978-94-009-4536-4\\_5](https://doi.org/10.1007/978-94-009-4536-4_5), 1986.

Lang, H. and Braun, L.: On the information content of air temperature in the context of snow melt estimation, *IAHS*, 190, 347–354, 1990.

Lawrence, M. G.: The Relationship between Relative Humidity and the Dewpoint Temperature in Moist Air: A Simple Conversion and Applications, *Bull. Amer. Meteor. Soc.*, 86, 225–234, <https://doi.org/10.1175/BAMS-86-2-225>, 2005.

Lehning, M., Bartelt, P., Brown, B., and Fierz, C.: A physical SNOWPACK model for the Swiss avalanche warning, *Cold Regions Science and Technology*, 35, 169–184, [https://doi.org/10.1016/S0165-232X\(02\)00072-1](https://doi.org/10.1016/S0165-232X(02)00072-1), 2002.

Liu, Y., Tan, Q., and Pan, T.: Determining the Parameters of the Ångström-Prescott Model for Estimating Solar Radiation in Different Regions of China: Calibration and Modeling, *Earth and Space Science*, 6, 1976–1986, <https://doi.org/10.1029/2019EA000635>, 2019.

Luo, Y., Arnold, J., Liu, S., Wang, X., and Chen, X.: Inclusion of glacier processes for distributed hydrological modeling at basin scale with application to a watershed in Tianshan Mountains, northwest China, *Journal of Hydrology*, 477, 72–85, <https://doi.org/10.1016/j.jhydrol.2012.11.005>, 2013.

Lutz, A. F., Immerzeel, W. W., Kraaijenbrink, P. D. A., Shrestha, A. B., and Bierkens, M. F. P.: Climate Change Impacts on the Upper Indus Hydrology: Sources, Shifts and Extremes, *PLoS ONE*, 11, e0165630, <https://doi.org/10.1371/journal.pone.0165630>, 2016.

MacDougall, A. H., Wheler, B. A., and Flowers, G. E.: A preliminary assessment of glacier melt-model parameter sensitivity and transferability in a dry subarctic environment, *The Cryosphere*, 5, 1011–1028, <https://doi.org/10.5194/tc-5-1011-2011>, 2011.

Marks, D., Domingo, J., Susong, D., Link, T., and Garen, D.: A spatially distributed energy balance snowmelt model for application in mountain basins, *Hydrol. Process.*, 13, 1935–1959, [https://doi.org/10.1002/\(SICI\)1099-1085\(199909\)13:12/13<1935::AID-HYP868>3.0.CO;2-C](https://doi.org/10.1002/(SICI)1099-1085(199909)13:12/13<1935::AID-HYP868>3.0.CO;2-C), 1999.

Marsh, C. B., Pomeroy, J. W., and Spiteri, R. J.: Implications of mountain shading on calculating energy for snowmelt using unstructured triangular meshes: Implication of Mountains shading for snowmelt, *Hydrol. Process.*, 26, 1767–1778, <https://doi.org/10.1002/hyp.9329>, 2012.

Martinec, J.: The degree-day factor for snowmelt-runoff forecasting, *IAHS Commission of Surface Waters*, 51, 468–477, 1960.

Martinec, J.: Snowmelt - runoff model for stream flow forecasts, *Nordic Hydrology*, 145–154, 1975.

Martinec, J., Rango, A., and Roberts, R.: *Snowmelt Runoff Model (SRM) User's Manual*, 180, 2008.

Masters, G. M.: *Renewable and efficient electric power systems*, John Wiley & Sons, Hoboken, NJ, 654 pp., 2004.

Matthews, T. and Hodgkins, R.: Interdecadal variability of degree-day factors on Vestari Hagafellsjökull (Langjökull, Iceland) and the importance of threshold air temperatures, *J. Glaciol.*, 62, 310–322, <https://doi.org/10.1017/jog.2016.21>, 2016.

McGinn, R. A.: Degree-day snowmelt runoff experiments; Clear Lake Watershed, Riding Mountain National Park, *Geographical Essays*, 15, 16, 2012.

Meeus, J.: *Astronomical algorithms*, 1st English ed., Willmann-Bell, Richmond, Va, 429 pp., 1991.

Monteith, J. L. and Unsworth, M. H.: *Principles of environmental physics: plants, animals, and the atmosphere*, 4th ed., Elsevier/Academic Press, Amsterdam ; Boston, 401 pp., 2013.

Muhammad, S., Tian, L., Ali, S., Latif, Y., Wazir, M. A., Goheer, M. A., Saifullah, M., Hussain, I., and Shiyin, L.: Thin debris layers do not enhance melting of the Karakoram glaciers, *Science of The Total Environment*, 746, 141119, <https://doi.org/10.1016/j.scitotenv.2020.141119>, 2020.

Murray, F. W.: On the Computation of Saturation Vapor Pressure, *J. Appl. Meteor.*, 6, 203–204, [https://doi.org/10.1175/1520-0450\(1967\)006<0203:OTCOSV>2.0.CO;2](https://doi.org/10.1175/1520-0450(1967)006<0203:OTCOSV>2.0.CO;2), 1967.

Musselman, K. N., Clark, M. P., Liu, C., Ikeda, K., and Rasmussen, R.: Slower snowmelt in a warmer world, *Nature Clim Change*, 7, 214–219, <https://doi.org/10.1038/nclimate3225>, 2017.

Oerlemans, J.: *Glaciers and climate change*, A.A. Balkema Publishers, Lisse ; Exton, (PA), 148 pp., 2001.

Pelkowski, J.: A physical rationale for generalized Ångström–Prescott regression, *Solar Energy*, 83, 955–963, <https://doi.org/10.1016/j.solener.2008.12.011>, 2009.

Pellicciotti, F., Brock, B., Strasser, U., Burlando, P., Funk, M., and Corripio, J.: An enhanced temperature-index glacier melt model including the shortwave radiation balance: development and testing for Haut Glacier d’Arolla, Switzerland, *J. Glaciol.*, 51, 573–587, <https://doi.org/10.3189/172756505781829124>, 2005.

Prasad, V. H. and Roy, P. S.: Estimation of Snowmelt Runoff in Beas Basin, India, *Geocarto International*, 20, 41–47, <https://doi.org/10.1080/10106040508542344>, 2005.

Quick, M. C. and Pipes, A.: U.B.C. Watershed model / Le modèle du bassin versant U.C.B, *Hydrological Sciences Bulletin*, 22, 153–161, <https://doi.org/10.1080/02626667709491701>, 1977.

Rango, A. and Martinec, J.: Application of a Snowmelt-Runoff Model Using Landsat Data, *Hydrology Research*, 10, 225–238, <https://doi.org/10.2166/nh.1979.0006>, 1979.

Rango, A. and Martinec, J.: Revisiting the degree-day method for snowmelt computations, *J Am Water Resources Assoc*, 31, 657–669, <https://doi.org/10.1111/j.1752-1688.1995.tb03392.x>, 1995.

Reda, I. and Andreas, A.: Solar position algorithm for solar radiation applications, *Solar Energy*, 76, 577–589, <https://doi.org/10.1016/j.solener.2003.12.003>, 2004.

Rensheng, C., Shihua, L., Ersi, K., Jianping, Y., and Xibin, J.: Estimating daily global radiation using two types of revised models in China, *Energy Conversion and Management*, 47, 865–878, <https://doi.org/10.1016/j.enconman.2005.06.015>, 2006.

Schaefli, B. and Huss, M.: Integrating point glacier mass balance observations into hydrologic model identification, *Hydrol. Earth Syst. Sci.*, 15, 1227–1241, <https://doi.org/10.5194/hess-15-1227-2011>, 2011.

Schmid, M.-O., Gubler, S., Fiddes, J., and Gruber, S.: Inferring snowpack ripening and melt-out from distributed measurements of near-surface ground temperatures, *The Cryosphere*, 6, 1127–1139, <https://doi.org/10.5194/tc-6-1127-2012>, 2012.

Schreider, S. Yu., Whetton, P. H., Jakeman, A. J., and Pittock, A. B.: Runoff modelling for snow-affected catchments in the Australian alpine region, eastern Victoria, *Journal of Hydrology*, 200, 1–23, [https://doi.org/10.1016/S0022-1694\(97\)00006-1](https://doi.org/10.1016/S0022-1694(97)00006-1), 1997.

Shea, J. M., Dan Moore, R., and Stahl, K.: Derivation of melt factors from glacier mass-balance records in western Canada, *J. Glaciol.*, 55, 123–130, <https://doi.org/10.3189/002214309788608886>, 2009.

Swinbank, W. C.: Long-wave radiation from clear skies, *Q.J Royal Met. Soc.*, 89, 339–348, <https://doi.org/10.1002/qj.49708938105>, 1963.

Tahir, A. A., Chevallier, P., Arnaud, Y., and Ahmad, B.: Snow cover dynamics and hydrological regime of the Hunza River basin, Karakoram Range, Northern Pakistan, *Hydrol. Earth Syst. Sci.*, 15, 2275–2290, <https://doi.org/10.5194/hess-15-2275-2011>, 2011.

USACE: Snow hydrology: Summary report of the snow investigations, 1956.

USACE: Runoff from Snowmelt, 1998.

Vincent, C. and Thibert, E.: Brief communication: Nonlinear sensitivity of glacier-mass balance attested by temperature-index models, *Glaciers/Alpine Glaciers*, <https://doi.org/10.5194/tc-2022-210>, 2022.

Walter, M. T., Brooks, E. S., McCool, D. K., King, L. G., Molnau, M., and Boll, J.: Process-based snowmelt modeling: does it require more input data than temperature-index modeling, *Journal of hydrology*, v. 300, 65–75, 2005.

Warren, S. G.: Optical properties of snow, *Rev. Geophys.*, 20, 67, <https://doi.org/10.1029/RG020i001p00067>, 1982.

Warren, S. G. and Wiscombe, W. J.: A Model for the Spectral Albedo of Snow. II: Snow Containing Atmospheric Aerosols, *J. Atmos. Sci.*, 37, 2734–2745, [https://doi.org/10.1175/1520-0469\(1980\)037<2734:AMFTSA>2.0.CO;2](https://doi.org/10.1175/1520-0469(1980)037<2734:AMFTSA>2.0.CO;2), 1980.

Wheler, B. A.: Glacier melt modelling in the Donjek Range, St. Elias Mountains, Yukon Territory, M.S. thesis, Dept. of Earth Sciences, Simon Fraser University, 283 pp, 2009.

Wiscombe, W. J. and Warren, S. G.: A Model for the Spectral Albedo of Snow. I: Pure Snow, *J. Atmos. Sci.*, 37, 2712–2733, [https://doi.org/10.1175/1520-0469\(1980\)037<2712:AMFTSA>2.0.CO;2](https://doi.org/10.1175/1520-0469(1980)037<2712:AMFTSA>2.0.CO;2), 1980.

Yang, K. and Koike, T.: A general model to estimate hourly and daily solar radiation for hydrological studies: GENERAL SOLAR RADIATION, *Water Resour. Res.*, 41, <https://doi.org/10.1029/2005WR003976>, 2005.

Zhang, Y., Liu, S., Xie, C., and Ding, Y.: Application of a degree-day model for the determination of contributions to glacier meltwater and runoff near Keqicar Baqi glacier, southwestern Tien Shan, *Ann. Glaciol.*, 43, 280–284, <https://doi.org/10.3189/172756406781812320>, 2006.

Zingg, T.: Beziehung zwischen Temperatur und Schmelzwasser und ihre Bedeutung für Niederschlags- und Abflussfragen., Publication of Association of Hydrological Sciences, 32, 266–269, 1951.